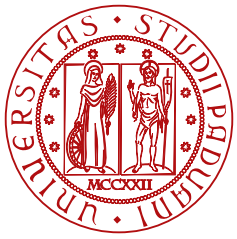

UNIVERSITÀ DEGLI STUDI DI PADOVA

Dipartimento di Fisica e Astronomia Galileo Galilei

# UNIVERSITÀ DEGLI STUDI DI PADOVA

**Dipartimento di Fisica e Astronomia "Galileo Galilei"**

**Master Degree in Physics of Data**

**Final Dissertation**

# Mission Planning for Earth Observation: a Tree Tensor Network approach


**Thesis supervisor**

**Dr. Siloi Ilaria**

**Thesis co-supervisor**

**Prof. Montangero Simone**

**Catuogno Tommaso**

**Candidate**

**De Masi Michele**


**Academic Year 2023-2024**

# Abstract

The mission planning (MP) is a crucial aspect of Earth Observation (EO) that targets the optimal scheduling of satellites' orbits for the data collection of Earth information upon end-users' requests. This task is a complex combinatorial problem that involves the optimization of a set of variables, describing both the acquisition of target images of the Earth's surface and the subsequent downloading of the acquired information to ground stations. The MP problem can be formulated as a knapsack problem (NP-hard problem), where the cost function consists of binary variables, whose optimal configuration provides the time-ordered shortlist of the possible observations and downlinks - the planned mission - according to some selected constraints. This Thesis represents the output of a six-month internship within the research division of Thales Alenia Space Italia (TASI). Starting from a mathematical formulation of the MP problem provided by TASI, we first map the original classical problem into a ground-state search for the corresponding quantum many-body Hamiltonian, reminiscent of spin glass models. We then explore the feasibility of reaching the optimal solution for a representative set of small problem instances using quantum-inspired algorithms based on Tree Tensor Networks (TTN), which allow for an efficient representation of the ground state of many body systems. This study concludes with a comparison to a Quadratic Program (QP) classical solver.

# Contents

# List of Figures

# List of Tables

# Introduction

Many problems of theoretical and practical relevance can be framed as combinatorial optimization problems over discrete configuration spaces, where the goal is determining the optimal arrangement of discrete variables to maximize or minimize a designated objective function. Their application spans across various domains, including graph theory, where optimization techniques serve as finding the shortest path between the nodes, network flow maximization, and minimizing traversal costs. Of notable interest are quadratic unconstrained binary optimization (QUBO) problems, appearing in diverse fields such as machine learning, materials design, software verification, flight traffic control, constraint satisfaction problems, portfolio management, and logistics. Enhancing our capability in effectively addressing real-world problems, especially those concerning operational planning and scheduling, represents a promising avenue for potential breakthroughs in emerging computational paradigms, such as quantum computing. Classical approaches to such problems often rely on heuristic methods, which may lack performance guarantees or runtime efficiency. Even marginal enhancements in the solution quality can impact resource costs including time and energy consumption required for practical solution implementation.

This Thesis represents the output of a six-month internship with the research division of Thales Alenia Space Italia (TASI), whose main scope is studying and solving problems in the Earth Observation (EO) scenario. Earth observation refers to the use of remote technologies to monitor land, atmosphere, seas, rivers, and lakes. The monitoring is performed by ground-state stations or satellites, and the acquisition of images and high-resolution data provides valuable information on Earth processes, thus enabling global monitoring for applications ranging from climate monitoring and natural resource management to disaster response and urban planning. In this context, constellations of satellites continuously acquire data from the Earth, but this process has limitations due to the different factors, such as the organization of the mission for the constellations, the data acquisitions, the processing of the raw data and the analysis of them.

This Thesis focuses on the solution of optimization problems related to the scheduling of the satellites mission and the raw data acquisition, which is defined as *Mission Planning* (MP) prob-

lem. MP specifically refers to the scheduling of satellites observations to fulfil a given list of acquisition requests in a certain time horizon, from one day to a few days. The mathematical formulation of the MP problem resides in those problems defined as combinatorial problems, whose computational complexity is known to be NP-hard [1]. Specifically, we consider a mathematical formulation of the MP problem in terms of the *knapsack problem* [2], where the optimal mission accounts for all the users requests while fulfilling other operational constraints.

Possible classical approaches to solve this type of problems are Linear Programming Solvers, as *Dynamic Programming*[2], *Greedy algorithm*[3], *Branch and Bound*[4], approximation algorithms [5] and metaheuristic algorithms [6]–[8]. With the advent of quantum computing [9], [10], other approaches based on quantum algorithms have become available. This is the case of quantum annealing, where the solution of the combinatorial problem is obtained by adiabatically preparing the ground state of the corresponding Ising Hamiltonian, or Quantum Neural Networks, in which a classical machine learning algorithms is adapted to run on a quantum computer[11].

The strategy employed for this Thesis is to apply methods based on quantum physics which operate on classical computers, specifically, Tensor Network (TN) methods [12]. In quantum many-body physics, TN numerical techniques have been developed to represent the states of quantum many-body problems [13]. The underlying idea involves decomposing a wave function into local tensors connected by bonds. Each tensor captures the local entanglement structure within a subsystem, while the bonds encode the correlations between neighboring subsystems. This arrangement is achieved by organizing the tensors into a hierarchical configuration, where the entanglement between distinct regions is captured through the auxiliary indices connecting the tensors. The level of information captured can be regulated by the *bond dimension* $\chi$.

This thesis introduces the optimization of the Mission Planning problem using a specific ansatz for the wavefunction, namely the Tree Tensor Network (TTN) ansatz. Starting by defining in-depth Earth Observation, characterized by different use cases in which it is divided, the chapter 1 has the aim to strictly explain the Mission Planning problem for Earth Observation, giving an overview of the challenge. Consequently, in Sec.1.2, the mathematical formulation of the Mission Planning is explored, introducing essential parameters and the considered Constraints, important to define the objective function that must be minimized. Subsequently, in Sec. 1.3, the problem is transformed into a QUBO problem, accompanied by a concise explanation of what QUBO problems entail. Finally, in sec.1.4, the quadratic formulation is mapped onto an Ising-like Hamiltonian, which is the final formulation used to apply the TTN approach.

The chapter 2, gives an explanation of quantum many-body problems (sec. 2.1), more specifically focusing into Ising Spin-glasses models, sec.2.2. After a little introduction of Exact Di-

agonalitazion techniques in sec. 2.3, the entanglement in quantum system is explained (sec. 2.4). Finally, the Tensor Network methods are introduced, given an overview of their property, required to introduce the Tree Tensor Network ansatz, sec. 2.5.

Chapter 3 begins by providing an overview of the mission planning instances and the desired outcomes of interest, namely the mission plan, the fulfilled constraints and the mission cost. The exploration begins with an examination of how the bond dimension impacts the ground-state search for small systems ($N = 16$,32,64), demonstrating the direct correlation between the energy convergence behaviour and the bond dimension. As the mission planning problem is a classical NP-hard problem characterized by an exponential number of local minima, an additional transverse field is incorporated into the MP Hamiltonian within the framework of the TTN approach, aiming to facilitate escape from local minima. To assess the effectiveness of this field, two systems are scrutinized through iterative random initializations, a pivotal aspect of the algorithm. After demonstrating the effects of this field, further instances are considered, encompassing various system sizes ranging from $N = 16$ to $N = 1024$ and comparing the TTN results with a classical solver.

In the concluding chapter 4, all significant points will be summarized. It will be shown that the TTN optimization algorithm, implemented in the Quantum Green Tea library, can be an optimal approach for the analyzed instances. Particularly, our results show that an additional transverse field applied to the MP Hamiltonian helps to escape from local minima, increasing the probability to find the ground state. Considering the purpose of the mission planning, we then focus on the mission quality, that is the accuracy of the satisfied constraints. To have a comparison with a classical solver, the outcomes obtained by the TTN algorithm are compared with the solution of the CPLEX solver, which have similar, almost identical, solutions in terms of satisfied constraints, when considering instances with at most 256 qubits. Instead, the computational time to reach the optimal solution is significantly worse for the TTN algorithm. Finally, to push the limit of our implementation other instances with 512 and 1024 qubits are taken into account, showing that the TTN maintains stability in terms of quality of the mission.

# 1 Mission Planning for Earth Observation

*This chapter is dedicated to the Mission Planning problem within the framework of Earth Observation. Sec. 1.1 begins with the definition and an in-depth analysis of Earth Observation, encompassing its significance, various Use Cases, and the nuanced subdivision into various issues and aspects. By scrutinising Earth Observation from multiple angles, we gain valuable insights that pave the way for a focused examination of the challenges and considerations inherent in Mission Planning. Sec. 1.2 then explores the mathematical formulation of the Mission Planning problem, introducing essential parameters and Constraints necessary for this formulation, providing a comprehensive overview. This Constraints are explained highlighting their significance and the underlying equations used to describe them. With the understanding of Mission Planning and its formulation established, Sec.1.3 offers an introduction of the Quadratic Unconstrained Binary Problem (QUBO), providing a comprehensive overview of QUBO's importance within this context and its significance in relation to Mission Planning. Such insights are valuable for transforming this problem into an Ising-like Hamiltonian, explained in Sec.1.4.*

## 1.1 The Earth Observation challenge

Earth Observation (EO) is gathering data on the Earth's physical, chemical and biological systems, using remote sensing technologies. This activity can be performed by remote technologies, such as satellites or ground-based platforms, such as weather stations. Aligned with the investigation conducted by *Thales Alenia Space Italia* (TASI), this thesis will focus on the satellite perspective. Through satellites, Earth Observation involves the utilization of satellite-mounted payloads to acquire imaging data that capture the Earth's characteristics. Earth observation images provide a global outlook, capturing large-scale phenomena with precision and completeness, which would require a substantial number of ground-level observers to achieve. Long-term, continuous monitoring of the environment of the Earth will allow a reliable assessment of the worldwide repercussions of human activities and the future scope of climate change expected. Examples of what types of data are extracted by Earth observation are surface thermal data, through termed optical instruments, recording the reflecting energy coming from the Sun across various wavelengths, including visible light and invisible infrared bands[14][15]. Typically, Earth Observation presents itself as a multifaceted challenge that encompasses various *Scenarios*, each delineating a specific Use Case (UC). These Scenarios, for satellite-based EO missions, span mission analysis, data acquisition, processing, and data analysis. The integration of these scenarios is depicted in Fig.1.1. illustrating the four phases that encapsulate the essence of EO in terms of the tasks at hand, where these phases are depicted alongside a distribution of the identified scenarios.

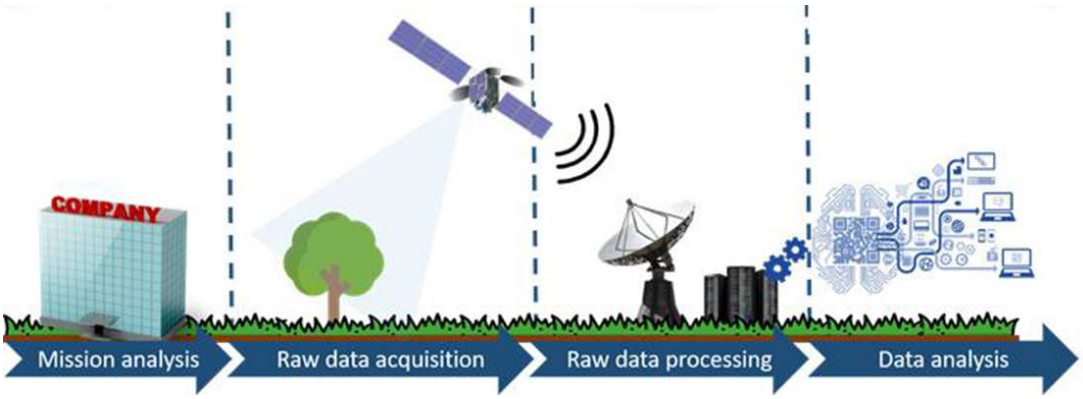


Figure 1.1: Steps of the Earth Observation, with the percentages representing the proportion of identified scenarios corresponding to each phase.

Various studies are conducted for each phase of the EO problem, with the aim of maximising the efficiency of each component. However, this thesis focuses solely on the initial two phases: mission analysis and raw data acquisition. The accomplishment of these tasks strongly depends on the optimal scheduling of satellite observations.

Nowadays, satellites have become powerful scientific tools and they continuously acquire images of our planet from orbit. Typically, missions for collecting earth images involves constellations of satellites ($\sim$10), which are appealing for their robustness and flexibility, especially in adapting to expected and unexpected events. Despite their excellent capabilities, when considering how to schedule a mission of a constellation of satellites, other considerations must be addressed, such as limitations from various sources of nature, economic, and manufacturing. There are also limitations related to time, memory, and other aerospace considerations that must be addressed. Then, it is essential that satellite deployment is efficient, ensuring optimal use. This challenge is known as the satellite *Mission Planning* (MP) problem. The purpose of mission planning is to optimise the scheduling of satellite observations to fulfil a given list of user requests in a certain time horizons, which can vary from one day to few days. Current approaches to this problem are based on both deterministic and metaheuristic algorithms, capable of generating optimal solutions for the current constellation of a few satellites [16]. However, a growing trend involves the deployment of extensive constellations of small satellites ($\sim$100), making the identification of an optimal solution to the mission planning problem increasingly challenging, even for short planning time horizons. The emerging extensive satellite constellations are becoming increasingly intricate, especially with the implementation of the Inter-Satellite Link (ISL). This technology enables satellite-to-satellite communication, creating a network where satellites can share information, without the need, for the satellites which makes the acquisition, to orbit over a ground station for data download. Then, the goal of the mission planning algorithm is to reduce the system's response time, particularly the delay from when a user request is submitted to when the product is downloaded, by evenly distributing tasks among the satellites that are accessible.

## 1.2 Mathematical formulation

The objective of Mission Planning for Earth Observation is to devise an efficient solution for managing the resources of the constellation to fulfil mission objectives. This involves optimizing the scheduling of satellite observations for a given list of user requests. These user requests involve capturing specific information of a specific target, such as specific area of the Earth's surface. A given set of these targets, called *Acquisition Requests* (ARs), must be fulfilled during the EO mission. This problem is described by two type decision variables, "*data take opportunities*" (DTOs), which refer to instances when each satellite has the opportunity to capture a specific AR at various times during the mission timeframe. These opportunities are characterized by the instantaneous time in which the acquisition can occur. The "*downlink opportunities*" (DLOs), which describes the transmission of acquired information from the individual satellite to receptive ground stations. Each satellite is constrained by limited onboard storage capacity, necessitating compactness to mitigate satellite launch costs and other manufacturing considerations. In addition, storing data onboard poses significant challenges, causing the need to optimize the *downlink* of acquired targets to ground stations. The DLOs represents the list of possible occasions on which each satellite can download this information.
The optimizer generates a list of feasible observations and downlinks by considering various constraints. This Mission Planning problem can be described by the following cost function:

$$\begin{aligned} C(\vec{x},\vec{y}) &= \sum_{i=1}^{N}\sum_{j=1}^{M}\sum_{k=1}^{\theta_{i,j}}\left(\alpha t_{i,j}^{k} x_{i,j}^{k} - \frac{\gamma}{M} x_{i,j}^{k}\right) + \sum_{i=1}^{N}\sum_{j=1}^{M}\sum_{r=1}^{\sigma_i}\left(\beta s_{i,j}^{r} y_{i,j}^{r}\right) = \\ &= \sum_{i=1}^{N}\sum_{j=1}^{M}\sum_{k=1}^{\theta_{i,j}} \alpha_{i,j}^{k} x_{i,j}^{k} + \sum_{i=1}^{N}\sum_{j=1}^{M}\sum_{r=1}^{\sigma_i} \beta_{i,j}^{r} y_{i,j}^{r}, \end{aligned} \tag{1.1}$$

and must be minimized with respect to the $\vec{x}$ and $\vec{y}$, which describe the DTOs and DLOs, respectively. The $\alpha_{i,j}^{k}$ and $\beta_{i,j}^{r}$ represent the inclusion of weights and temporal aspects. When $x_{i,j}^{k}$ is equal to 1, the *i-th* satellite acquires the *j-th* target at the *k-th* occurrence, it is 0 if it is not acquired; similarly, $y_{i,j}^{r}$ is equal to 1 if the *i-th* satellite schedules the downloading of the *j-th* acquired target at the *r-th* opportunity, or 0 otherwise.

$$\begin{cases} x_{i,j}^{k} = 1 & \text{acquisition completed} \\ x_{i,j}^{k} = 0 & \text{otherwise} \end{cases} \qquad \begin{cases} y_{i,j}^{r} = 1 & \text{download completed} \\ y_{i,j}^{r} = 0 & \text{otherwise} \end{cases} \tag{1.2}$$

The cost function, Eq. 1.1, is characterized by the following parameters:

- $N \in \mathbb{N}$: the number of satellites in the constellation;
- $M \in \mathbb{N}$: the number of acquisition requests characterizing the mission;
- $\theta_{i,j} \in \mathbb{N}$: the number of possible opportunities in which satellite *i* can acquire target *j*;
- $\sigma_i \in \mathbb{N}$: the number of possible opportunities in which satellite *i* can perform the downlink of an acquired target;
- $t^k_{i,j} \in \mathbb{R}$: instantaneous time in which satellite *i* acquires target *j* at the opportunity *k*;
- $s^r_{i,j} \in \mathbb{R}$: instantaneous time in which satellite *i* perform the downlink of target *j* at the opportunity *r*;
- $\alpha,\beta,\gamma \in \mathbb{R}$: weights associated with the problem.

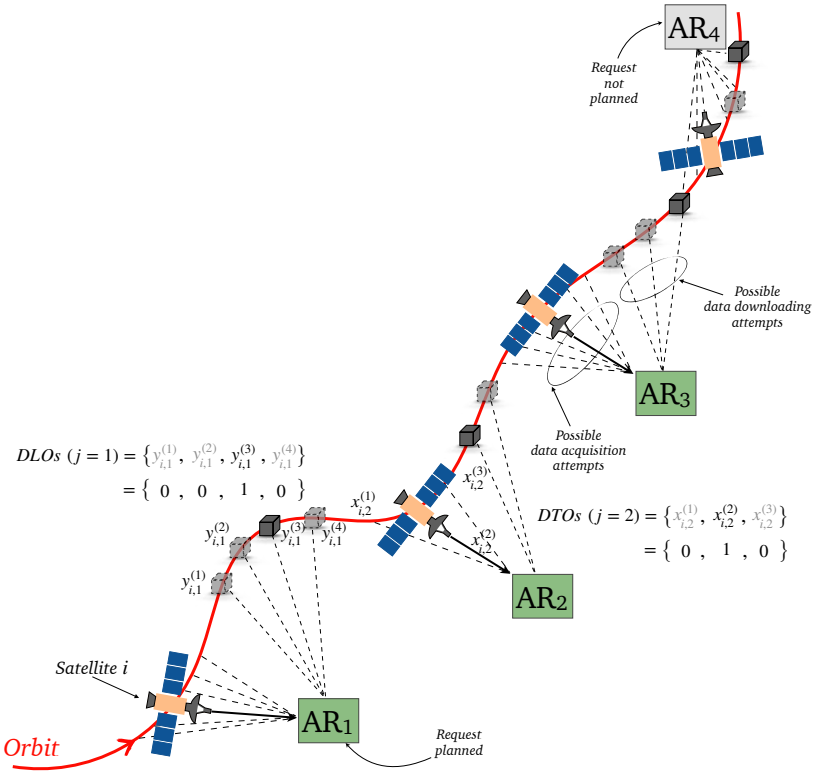


Figure 1.2: Visualization of the mission planning problem is depicted graphically. Each satellite $i$ is presented with multiple chances to capture the requested scene (AR) and subsequently transfer them due to memory constraints. Mission planning focuses on determining the most efficient schedule for these data acquisition requests.

As illustrated in the Fig.1.2, a typical satellite $i$ assigned the duty of acquiring $M$ ARs during its orbit. The dashed lines directly connected to the satellite represent the opportunities $\theta_{i,j}$ for the $i$-th satellite to acquire the $j$-th AR, i.e. the DTOs. Meanwhile, the dashed line connected to the gray cube signifies the possible data downlink attempts $\sigma_i$ for the $i$-th satellite.
The goal of an algorithm, designed to solve the MP problem, is to find $\vec{x}$ and $\vec{y}$ that minimize Eq.1.1, more specifically:

$$arg\min_{\vec{x},\vec{y}} C(\vec{x},\vec{y}) + \Omega_E/I, \tag{1.3}$$

where $\Omega_E$ is the set of constraints representing the problem. Moreover, while the equation 1.1 presents a fundamental aspect, the main complexity of this problem arises from the need to minimize it, taking into account a multitude of constraints. These constraints play a crucial role in shaping the solution space and ensuring that the resulting schedule meets all the necessary criteria and requirements. For this work, the applied constraints are:

1. One acquisition attempt per target:

$$\sum_{i=1}^{N}\sum_{k=1}^{\theta_{i,j}} x_{i,j}^{k} - 1 = 0 \qquad \forall j \in [1,M], \tag{1.4}$$

2. One download attempt per target:

$$\sum_{i=1}^{N}\sum_{r=1}^{\sigma_i} y_{i,j}^{r} - 1 = 0 \qquad \forall j \in [1,M], \tag{1.5}$$

3. Each acquisition must be downloaded:

$$\sum_{k=1}^{\theta_{i,j}} x_{i,j}^{k} - \sum_{r=1}^{\sigma_i} y_{i,r}^{r} = 0 \qquad \forall i \in [1,N], \quad \forall j \in [1,M], \tag{1.6}$$

4. Target acquisition precedes download:

$$\sum_{k=1}^{\theta_{i,j}} x_{i,j}^{k} t_{i,j}^{k} - \sum_{r=1}^{\sigma_i} y_{i,j}^{r} s_{i,j}^{r} \leq 0 \qquad \forall i \in [1,N], \quad \forall j \in [1,M], \tag{1.7}$$

5. Sufficient preparation time between two acquisitions:

$$\begin{aligned} x_{i,s}^{k} p_{i,s}^{k} - |x_{i,s}^{k} t_{i,s}^{k} - x_{i,j}^{k'} t_{i,j}^{k'}| \leq 0 \qquad & \forall i \in [1,N], \quad \forall j,s \in [1,M], \\ & \forall k \in [1,\theta_{i,s}], \quad \forall k' \in [1,\theta_{i,j}], \end{aligned} \tag{1.8}$$

6. Sufficient preparation time between two downlinks:

$$y^r_{i,g} d^r_{i,g} - |y^r_{i,g} s^r_{i,g} - y^{r'}_{i,j} s^{r'}_{i,j}| \leq 0 \qquad \begin{array}{l} \forall i \in [1,N], \quad \forall j,g \in [1,M], \\ \forall r \in [1,\sigma_i], \quad \forall r' \in [1,\sigma_i]. \end{array} \tag{1.9}$$

Where other parameters are introduced:

- $p^k_{i,j} \in \mathbb{R}$: the preparation time of the *i-th* satellite to gain *j-th* target at *k-th* occurrence;
- $d^r_{i,j} \in \mathbb{R}$: the preparation downlink time of the *i-th* satellite to download *j-th* target at *r-th* occurrence.

In table 3.1, there are described some realistic range of value, which we aspect they can be associated to the Mission planning in coming years. Involving a large number of variables to be optimized, considering and satisfying numerous constraints, make this task really challenging. However, the focus of this thesis lies on approaching this problem from a novel perspective, with the aim of identifying an optimal solution.

| **Realistic range of variables and parameters** | | | |
|---|---|---|---|
| Parameter ID | Description | Domain | Range Values |
| N | number of satellites | $\mathbb{N}$ | [1-1000] |
| M | number of ARs | $\mathbb{N}$ | [200-50k] |
| $\theta_{i,j}$ | number of DTOs | $\mathbb{N}$ | [2-50] |
| $\sigma_i$ | number of DLOs | $\mathbb{N}$ | [10-100] |
| $t^k_{i,j}$ | Instant acquisition time | $\mathbb{R}$ | [1hr-few days] |
| $s^r_{i,j}$ | Instant downlink time | $\mathbb{R}$ | [1hr-few days] |
| $p^k_{i,j}$ | Preparation time after one acquisition | $\mathbb{R}$ | [10 sec - 60 sec] |
| $d^k_{i,j}$ | Preparation time after one downlink | $\mathbb{R}$ | [10 sec - 60 sec] |

Table 1.1: Information on the realistic range of variables and parameters in the mathematical model

## 1.3 QUBO formulation

The MP problem, due to its limitation and definition, belongs to the so-called *knapsack* problem. The knapsack problem is a classic combinatorial optimization problem where the goal is to maximize the value of items selected to fit within a given weight constraint of a knapsack. Similarly, in the mission planning problem, we are required to maximize the number of ARs within a given horizon time. For this reason, the cost function targets the arrangement of binaries that minimize the time (mission cost) while satisfying the constraints [17]. Different classical models and algorithms can be implemented to solve knapsack problems, as *Dynamic Programming*[2], *Greedy algorithm*[3], *Branch and Bound*[4], approximation algorithms [5] and metaheuristic algorithms [6]–[8].
The objective of this study is to apply a different approach to find a solution to the Mission Planning (MP) problem, as defined in Equation 1.1, by employing techniques drawn from many-body physics, notably tensor network methods. To accomplish this, it is first necessary to reframe the existing mathematical formulations into a *quadratic unconstrained binary optimization* (QUBO) problem [18]. QUBO serves as a unified model capable of representing a wide range of combinatorial optimization problems [19][20].
QUBO problem represents challenging mathematical optimization tasks involving the minimization of a quadratic objective function:

$$f(\vec{x}) = \vec{x}^T Q \vec{x}, \tag{1.10}$$

where $\vec{x}$ is a vector of binary variables and $Q$ is a symmetric matrix. Here, $f : \mathbb{B}^n \Rightarrow \mathbb{R}$ is a *Pseudo-Boolean function*, with *n* a positive integer, $\mathbb{B} = \{0,1\}$ and $\mathbb{R}$ the set of real numbers[21]. These problems are known to be NP-hard, implying that finding an optimal solution generally requires exponential time with respect to the size of the problem. Where QUBO problem can be written as:

$$arg \min_{\vec{x} \in \mathbb{B}^n} f(\vec{x}) = arg \min_{\vec{x} \in \mathbb{B}^n} \left( \sum_{j=1}^{n} \sum_{k>j}^{n} Q_{j,k} x_j x_k + \sum_{j=1}^{n} Q_{jj} x_j \right). \tag{1.11}$$

However, when comparing the QUBO formulation, as represented by Equation 1.10, to the Mission Planning problem described by Equation 1.1, it becomes apparent that they share similarities, albeit without the consideration of previously introduced constraints. The objective of an algorithm tasked with minimizing the cost function is to find a solution that

adheres to the associated constraints. If the domain set of these constraints is denoted by $\Omega_E$, then the optimal solution must reside within this domain, that is, $\vec{x}_{opt} \in \Omega_E$, satisfying $f(\vec{x}_{opt}) \leq \vec{x} \quad \forall f(\vec{x}) \in \Omega_E$. Then it is important to incorporate the constraint into the QUBO formulation, usually achieved by converting a binary Integer Linear Programming (ILP) problem into a quadratic one. In this context, the ILP problems correspond to the constraints inherent in MP.

For the case of mission planning problem, the considered linear constraints can be categorised into two types: equality constraints and inequality constraints. Then the general quadratic problem is defined as:

$$\begin{cases} arg\min_{\vec{x}\in\mathbb{B}^n} f(\vec{x}) \\ C_{eq}\vec{x} = \vec{k}_{eq} \\ C_{in}\vec{x} \leq \vec{k}_{in} \end{cases} \tag{1.12}$$

For the equality constraints, such as the second equation in 1.12, it is feasible to convert $C_{eq}\vec{x}$ into a parameter that is dependent on $\vec{x}$, denoted as $c_{eq}^{m}(\vec{x})$ with $m = 1, \ldots, p$. Consequently, this leads to a set of equations defined as:

$$\{c_m^{eq}(\vec{x}) = \vec{k}_m^{eq}\}.$$

These set of equality constraints can be converted in a quadratic problem and incorporated into $f(\vec{x})$ as a term of penalty, expressed as:

$$P_m(\vec{x}) = \left(c_m^{eq}(\vec{x}) - \vec{k}_m^{eq}\right)^2. \tag{1.13}$$

Where,

$$\begin{cases} P_m(\vec{x}) = 0 \quad \vec{x} \quad \text{feasible} \\ P_m(\vec{x}) \geq 0 \quad \vec{x} \quad \text{infeasible} \end{cases} \tag{1.14}$$

In certain scenarios, achieving a zero value for these penalty terms might not be feasible; therefore, the objective is to minimize them as much as possible.

Now, considering the third equation in 1.12, which represents the inequality constraints, an analogous approach to the one used for the equality constraints needs to be identified. A collection of these constraints is specified as:

$$\{c_l^{in}(\vec{x}) \leq \vec{k}_l^{in}\},$$

where $l = 1, \ldots, q$. Which can be converted by a simple equality $c(\vec{x}) + s = k$, where $s \in \mathbb{N}$ and $s \leq k$. This gives the opportunity to define an inequality as a penalty terms for a quadratic problem:

$$P_l(\vec{x}) = \left(c_l^{in}(\vec{x}) + s_l - \vec{k}_l^{in}\right)^2. \tag{1.15}$$

Where,

$$s_l = \sum_{\alpha=0}^{m_l-1} 2^\alpha b_{l,\alpha} \quad \text{with} \quad m_l = \lfloor \log_2 k_l^{in} \rfloor + 1 \quad \text{and} \quad b_{l,\alpha} \in \mathbb{B}. \tag{1.16}$$

Then,

$$\begin{cases} P_l(\vec{x}) = 0 & \vec{x} \quad \text{feasible} \\ P_l(\vec{x}) \geq 0 & \vec{x} \quad \text{infeasible} \end{cases} \tag{1.17}$$

When dealing with a set of inequality constraints, there is a strategy to convert them into additional terms within the objective function $f(\vec{x})$. This adaptation might involve the introduction of additional *slack variables*, to supplement existing $N$ variables [19].
At the end, having converted the linear constraint into a quadratic problem, it is possible to rewrite a final objective function:

$$Obj(\vec{x}) = f(\vec{x}) + \sum_{m=1}^{p} \mu_m P_m(\vec{x}) + \sum_{l=1}^{q} \mu_l P_l(\vec{x}). \tag{1.18}$$

The parameters $\mu_l$ and $\mu_m$, being constraint prefactors greater than zero, hold pivotal roles in the objective function minimization process. Their values influence the degree of emphasis placed on individual constraints. By assigning suitable weights to these parameters, the optimization algorithm can effectively navigate towards an optimal solution that appropriately balances the competing objectives and constraints inherent in the problem.
To incorporate the constraints of the Mission Planning problem, reported previously in Sec.1.2, to the cost function 1.1, they can be reformulated as quadratic problems, as discussed earlier, to yield a final objective function represented as a QUBO problem.

The first three constraints, 1.4, 1.5 and 1.6, which are simple equalities, can be expressed as Eq.1.13, resulting in the following.

$$Eq.1.4 \quad \Rightarrow \quad C_{DTO}(\vec{x}) = \sum_{j=1}^{M} \left[ \sum_{i=1}^{N} \sum_{k=1}^{\theta_{i,j}} x_{i,j}^{k} - 1 \right]^2 . \tag{1.19}$$

$$Eq.1.5 \quad \Rightarrow \quad C_{DLO}(\vec{y}) = \sum_{j=1}^{M} \left[ \sum_{i=1}^{N} \sum_{r=1}^{\sigma_i} y_{i,j}^{r} - 1 \right]^2 . \tag{1.20}$$

$$Eq.1.6 \quad \Rightarrow \quad C_{ME}(\vec{x},\vec{y}) = \sum_{i=1}^{N} \sum_{j=1}^{M} \left[ \sum_{j=1}^{\theta_{i,j}} x_{i,j}^{k} - \sum_{r=1}^{\sigma_i} y_{i,j}^{r} \right]^2 . \tag{1.21}$$

For the remaining constraint, 1.7, 1.8 and 1.9, a different strategy is pursued. Introducing slack variables may not be the most efficient approach, as the incorporation of extra variables substantially escalates the computational time and intricacy of the problem, potentially hindering the optimization process. As reported by Kochenberger in [19], this type of inequality constraint, such as $x_i + x_j \leq 1$, is very common, and penalty terms can be written as a multiplication over them, $\mu x_i x_j$. For these three constraints, the inequality is determined by fixed parameters, such as predetermined instantaneous and preparation times. By processing these parameters, it becomes apparent which couple of binary variables cannot both be set to 1 simultaneously. Then, for the constraint (1.7), $y_{i,j}^{r}$ is allowed in conjunction with $x_{i,j}^{k}$ only if $t_{i,j}^{k} \leq s_{i,j}^{r}$. Then the forbidden domain is:

$$\mathbb{F}_{i,j} = \left\{ (r,k) \quad | \quad t_{i,j}^{k} > s_{i,j}^{r} \right\} . \tag{1.22}$$

Identical approach was employed to define the forbidden domains for constrains (1.8) and (1.9). Respectively:

$$\mathbb{G}_i = \left\{ (s,j,k,k') \quad | \quad p_{i,s}^{k} - |t_{i,s}^{k} - t_{i,j}^{k'}| > 0 \right\} , \tag{1.23}$$

$$\mathbb{J}_i = \left\{ (g,j,r,r') \quad | \quad d_{i,g}^{r} - |s_{i,g}^{r} - d_{i,j}^{r'}| > 0 \right\} . \tag{1.24}$$

Then, the penalty terms become:

$$Eq.1.7 \quad \Rightarrow \quad C_{AD}(\vec{x},\vec{y}) = \sum_{i=1}^{N} \sum_{j=1}^{M} \sum_{(k,r)\in\mathbb{F}_{i,j}} x_{i,j}^{k} y_{i,j}^{r}, \tag{1.25}$$

$$Eq.1.8 \quad \Rightarrow \quad C_{PDTO}(\vec{x},\vec{y}) = \sum_{i=1}^{N} \sum_{(s,j,k,k')\in\mathbb{G}_i} x_{i,s}^{k} x_{i,j}^{k'}, \tag{1.26}$$

$$Eq.1.9 \quad \Rightarrow \quad C_{PDLO}(\vec{x},\vec{y}) = \sum_{i=1}^{N} \sum_{(g,j,r,r')\in\mathbb{J}_i} y_{i,g}^{r} y_{i,j}^{r'}. \tag{1.27}$$

All of these, leads into a cost function defined by a QUBO problem, where each penalty is multiplied by a corresponding pre-factor:

$$\begin{aligned} C_{QUBO}(\vec{x},\vec{y}) = C(\vec{x},\vec{y}) + \lambda_1 C_{DTO}(\vec{x}) + \lambda_2 C_{DLO}(\vec{y}) + \\ + \lambda_3 C_{ME}(\vec{x},\vec{y}) + \lambda_4 C_{AD}(\vec{x},\vec{y}) + \\ + \lambda_5 C_{PDTO}(\vec{x},\vec{y}) + \lambda_6 C_{PDLO}(\vec{x},\vec{y}). \end{aligned} \tag{1.28}$$

## 1.4 Mapping into an Ising model

QUBO problems are recognized as NP-hard due to the significant amount of time required to find an optimal solution. NP-hard refers to a category of problems that are as hard as the most challenging problems in NP, where NP (Non-deterministic Polynomial time) comprises decision problems for which solutions can be verified efficiently. These problems do not necessarily belong to NP and may not even be decidable. One potential approach to solve NP-hard problems is through adiabatic quantum optimization (AQO), the logic behind using quantum algorithms, such as quantum annealing [22], [23], or numerical methods based on quantum physics, to solve hard optimization problems lies in reformulating the problem into a Hamiltonian, specifically an Ising-like Hamiltonian, known to be NP-hard for conventional computers [24], [25] and commonly referred to as a QUBO problem[26], [27]. By formulating an optimization problem as a QUBO problem, it becomes feasible to map it into an Ising-like Hamiltonian, as thoroughly explained by Lucas[1], converting the problem into a ground-state search of a quantum many-body Hamiltonian. The most important step consists of transforming the two binary variables into spin-$\frac{1}{2}$ variables:

$$\begin{aligned} x_{i,j}^k \in \{0,1\} \quad &\longrightarrow \quad \tau_{i,j}^k \in \{-1,1\}\,, \\ y_{i,j}^r \in \{0,1\} \quad &\longrightarrow \quad \nu_{i,j}^r \in \{-1,1\}\,. \end{aligned} \tag{1.29}$$

With the following transformations:

$$\left\{ \begin{array}{l} \tau_{i,j}^k = 1 - 2x_{i,j}^k \\ \nu_{i,j}^r = 1 - 2y_{i,j}^r \end{array} \right. \quad \longleftrightarrow \quad \left\{ \begin{array}{l} x_{i,j}^k = \frac{1}{2}\left(1 - \tau_{i,j}^k\right) \\ y_{i,j}^r = \frac{1}{2}\left(1 - \nu_{i,j}^r\right) \end{array} \right. \tag{1.30}$$

Applying these transformations to Eq.1.28 we obtain a classical Ising-like Hamiltonian:

$$\mathcal{H}_{MP}\left[\vec{\tau},\vec{\nu}\right] = Cte \times \mathbb{1} + \mathcal{H}_{SP}\left[\vec{\tau}\right] + \mathcal{H}_{SP}\left[\vec{\nu}\right] + \mathcal{H}_{INT}\left[\vec{\tau}\right] + \mathcal{H}_{INT}\left[\vec{\nu}\right] + \mathcal{H}_{INT}\left[\vec{\tau},\vec{\nu}\right]. \tag{1.31}$$

Where the second and third terms of Eq.1.31 represent the Ising magnetic fields terms:

$$\begin{aligned} \mathcal{H}_{SP}\left[\vec{\tau}\right] = &\sum_{i=1}^{N}\sum_{j=1}^{M}\sum_{k=1}^{\theta_{i,j}}\left[\frac{\sigma_i}{2}\left(\frac{\gamma}{M} - \alpha t_{i,j}^k\right) + \lambda_1\frac{1}{2}\left(\sum_{i'=1}^{N}\theta_{i',j} - 1\right) + \lambda_3\frac{1}{2}(\sigma_i + \theta_{i,j})\right]\tau_{i,j}^k \\ &- \sum_{i=1}^{N}\sum_{j=1}^{M}\sum_{k\in\mathbb{F}_{i,j}}\frac{1}{4}\lambda_4\tau_{i,j}^k - \frac{1}{4}\lambda_5\sum_{(s,j,k,k')\in\mathbb{G}_i}(\tau_{i,s}^k + \tau_{i,j}^{k'}), \end{aligned} \tag{1.32}$$

$$\begin{aligned}\mathcal{H}_{SP}\left[\vec{\nu}\right] =& \sum_{i=1}^{N}\sum_{j=1}^{M}\sum_{r=1}^{\sigma_i}\left[-\frac{1}{2}\beta\theta_{i,j}s_{i,j}^{r}+\lambda_2\left(1-\frac{3}{2}\sigma_i-\frac{1}{4}(N_2^{tot}-1)+N\sigma_i\right)+\right.\\ &\left.+\lambda_3\frac{1}{2}(\theta_{i,j}-\sigma_i)\right]\nu_{i,j}^{k}-\sum_{i=1}^{N}\sum_{j=1}^{M}\sum_{r\in\mathbb{F}_{i,j}}\frac{1}{4}\lambda_4\nu_{i,j}^{r}+\\ &-\frac{1}{4}\lambda_6\sum_{(g,j,r,r')\in\mathbb{J}_i}(\nu_{i,g}^{r}+\nu_{i,j}^{r'}).\end{aligned} \tag{1.33}$$

The last three therms of Eq.1.31 describe the interactions between spins:

$$\begin{aligned}\mathcal{H}_{INT}\left[\vec{\tau}\right] =& \sum_{i=1}^{N}\sum_{j=1}^{M}\left[\frac{1}{2}\left(\lambda_1+\lambda_3\right)\sum_{k=1}^{\theta_{i,j}}\sum_{k'>k}^{\theta_{i,j}}\tau_{i,j}^{k}\tau_{i,j}^{k'}+\frac{1}{2}\lambda_1\sum_{i'>i}^{N}\sum_{k=1}^{\theta_{i,j}}\sum_{k'=1}^{\theta_{i',j}}\tau_{i,j}^{k}\tau_{i',j}^{k'}\right]+\\ &+\frac{1}{4}\lambda_5\sum_{i=1}^{N}\sum_{(s,j,k,k')\in\mathbb{G}_i}\tau_{i,s}^{k}\tau_{i,j}^{k'},\end{aligned} \tag{1.34}$$

$$\begin{aligned}\mathcal{H}_{INT}\left[\vec{\nu}\right] =& \sum_{i=1}^{N}\sum_{j=1}^{M}\left[\frac{1}{2}\left(\lambda_2+\lambda_3\right)\sum_{r=1}^{\sigma_i}\sum_{r'>r}^{\sigma_i}\nu_{i,j}^{r}\nu_{i,j}^{r'}+\frac{1}{2}\lambda_2\sum_{i'>i}^{N}\sum_{r=1}^{\sigma_i}\sum_{r'=1}^{\sigma_{i'}}\nu_{i,j}^{r}\nu_{i',j}^{r'}\right]+\\ &+\frac{1}{4}\lambda_6\sum_{i=1}^{N}\sum_{(g,j,r,r')\in\mathbb{J}_i}\nu_{i,g}^{r}\nu_{i,j}^{r'},\end{aligned} \tag{1.35}$$

$$\mathcal{H}_{INT}\left[\vec{\tau},\vec{\nu}\right] = \sum_{i=1}^{N}\sum_{j=1}^{M}\left[-\frac{1}{2}\lambda_3\sum_{k=1}^{\theta_{i,j}}\sum_{r=1}^{\sigma_i}\tau_{i,j}^{k}\nu_{i,j}^{r}+\frac{1}{4}\lambda_4\sum_{(k,r)\in\mathbb{F}_{i,j}}\tau_{i,j}^{k}\nu_{i,j}^{r}\right], \tag{1.36}$$

The first term represent an *offset*, which is proportional to the identity:

$$\begin{aligned}Cte =& M(\lambda_1+\lambda_2)+\frac{1}{4}(3\lambda_3N^{tot}-2\lambda_1N_{DTO}^{tot}-2\lambda_2N_{DLO}^{tot})+\\ &+\sum_{i=1}^{N}\sum_{j=1}^{M}\left[\sum_{k=1}^{\theta_{i,j}}\left(\alpha t_{i,j}^{k}-\frac{\gamma}{M}\right)\sigma_i+\sum_{r=1}^{\sigma_i}\beta\theta_{i,j}s_{i,j}^{r}+\frac{1}{4}\lambda_1\theta_{i,j}(\theta_{i,j}-1)+\right.\\ &+\frac{1}{4}\lambda_2\sigma_i(\sigma_i-1)+\frac{1}{4}\lambda_3(\theta_{i,j}-\sigma_i)^2+\sum_{i'\neq i}^{N}\frac{1}{4}(\lambda_1\theta_{i,j}\theta_{i',j}+\lambda_1\sigma_i\sigma_{i'})+\\ &\left.+\lambda_4|\mathbb{F}_{i,j}|\right]+\sum_{i=1}^{N}\left[\lambda_5|\mathbb{G}_i|+\lambda_6|\mathbb{J}_i|\right].\end{aligned} \tag{1.37}$$

Where $N_{DTO}^{tot}$ and $N_{DLO}^{tot}$ are the numbers of DTO and DLO spins respectively, and $N^{tot}$ is the total number of spins.
However, the structure of this Hamiltonian resembles that of a spin-glass model. Which can be written in terms of Pauli matrices:

$$\mathcal{H} = \sum_{j=1}^{N^{tot}} h_j \sigma_j^z + \sum_{\langle j,k \rangle}^{N^{tot}} J_{j,k} \sigma_j^z \sigma_k^z + const. \tag{1.38}$$

Where $N$ is the number of variables, $h$ is the single-particle term corresponding to equations 1.32 and 1.33, **J** is the interaction term between spins, i.e. equations 1.34,1.35, and 1.36, and:

$$\hat{\sigma}_j^z \hat{\sigma}_k^z = \mathbb{1} \otimes \cdots \otimes \underset{\text{j-th}}{\sigma_z} \otimes \cdots \otimes \underset{\text{k-th}}{\sigma_z} \otimes \cdots \otimes \mathbb{1}. \tag{1.39}$$

In the current context, the original optimization problem revolves around determining the ground state of the Hamiltonian 1.31. This involves minimizing the original cost function, Eq.1.1, with all the constraints considered. By accessing the eigenstate with the lowest energy, the spin orientation is discerned, enabling the extraction of a bit string that delineates the Mission plan.

# 2 Method

*This Chapter is focused on exact and approximated methods to address the so-called many body problem. The section commences with a brief explanation of the many-body problem, specifically focusing on the Ising spin-glass model (sec. 2.1), as the Hamiltonian describing the mission planning problem belongs to this class of problems. After reviewing how to compute the exact spectrum of the Ising Hamiltonian (Sec.2.3), a brief discussion of the Entanglement for quantum many-body systems, sec.2.4. Subsequently, the Chapter delves into tensor networks methods (Sec. 2.5), employing a Tree Tensor Network configuration for the system, that allows the exploration of larger system sizes.*

## 2.1 The Many-Body problem

The quantum many-body problem refers to the study of several interacting quantum degrees of freedom composing a quantum system, and it is transversal to multiple scientific domains such as Condensed Matter Physics, Quantum Chemistry, and Atomic and Nuclear Physics[12]. The challenges of the quantum many body problem arises from the exponential growth of Hilbert space with the system size. The total Hilbert space of an N-body system is the tensor product of N single-body or local Hilbert spaces:

$$H_T = H_1 \otimes \cdots \otimes H_N. \tag{2.1}$$

The single-body constituents of the system can be any quantum degree of freedom. Chosen a basis for each constituent $\{|\alpha_j\rangle\}$, $j = 1, \ldots, \dim(H_j)$, a general state in $H_T$ can be represented as:

$$\psi = \sum c_{\alpha_1,\alpha 2,\ldots,\alpha_N} |\alpha_1,\alpha_2,\ldots,\alpha_N\rangle. \tag{2.2}$$

In the following we will work in the computational basis: the local basis are the the states of the Pauli matrix $\sigma_z$ namely,

$$|\alpha_j\rangle = \{|0\rangle,|1\rangle\}.$$

Assuming that the local dimension of each single body is $d$, then size of the total Hilbert space is $d^N$. Then the number of coefficients needed to express a general state is $d^N$. This means that this problem is extremely hard to attack numerically. For this reason, the exact computation of a quantum many-body problem poses significant challenges due to the extensive memory and time resources it demands. Consequently, researchers have turned to a variety of numerical approximation methods to tackle such complexities. These include mean-field theory, Monte Carlo methods, renormalization group techniques, and tensor network approaches. [12]

## 2.2 Spin-Glass models

Spin glasses are a class of disordered materials that exhibit complex behaviors due to the interplay of competing interactions among their constituent [28]. Spin glasses represent a diverse class of materials beyond simple alloys such as the Au-Fe system. Another example is the dilute magnetic semiconductor, where magnetic ions are sparsely distributed within a non-magnetic host lattice. In these materials, such as GaMnAs, the presence of magnetic ions introduces disorder into the system, leading to the formation of a spin glass state. The random distribution of magnetic ions results in frustration and competing magnetic interactions, akin to those found in alloy systems. Unlike conventional magnets, where magnetic moments align to produce ordered magnetic states, spin glasses possess a disordered arrangement of spins, similar to the randomness found in amorphous solids like glass. This disorder stems from the presence of competing magnetic interactions, resulting in frustration and the absence of a well-defined magnetic ground state. As the strength of the interaction between magnetic moments depends on their random distance, a spin glass can be understood as a magnetic system with randomly distributed interactions. The first mathematical formulation of this problem is by S. Edward and P. Anderson [29]:

$$\mathcal{H} = -\sum_{\langle j,k\rangle} J_{j,k} S_j S_k. \tag{2.3}$$

The local magnetic moments are represented by Ising spins $S_i = \pm 1$. **J** is the coupling matrix, whose entries are non-zero when lattice $j$ and $k$ are interacting, and the sum over $\langle j,k\rangle$ refers to

the sum over neighboring lattice points $j$ and $k$.
From this formulation it is clear the connection to the Ising model that plays a central role in providing a first understanding of magnetic phenomena. The general expression for an Ising model is as follows.

$$\mathcal{H}_{Ising} = \sum_i h_i S_i + \sum_{\langle i,j \rangle} J_{ij} S_i S_j, \tag{2.4}$$

where $h_i$ is a local field applied on each site and the bracket $\langle i,j \rangle$ are neighboring spins in the chosen lattice geometry. Clearly, the lattice geometry affects the interaction pattern. In the case where the system is described by graph $\mathcal{G} = (V,E)$, with $V$ denoting the system's degrees of freedom (nodes) and $E$ representing the interactions among them (edges), the previous Hamiltonian differs only on the sum indices, becoming a sum over the graph edges. Then the general Ising Hamiltonian for a general graph is:

$$\mathcal{H}_{graph} = \sum_i h_i S_i + \sum_{i,j \in E(\mathcal{G})} J_{ij} S_i S_j. \tag{2.5}$$

Being interested in a lattice system with local dimension 2, to represent the spin-$\frac{1}{2}$ variables, the $S_i$ interaction terms, in the Ising Hamiltonian, represent the z-component of the Pauli matrix. Then, a Hamiltonian of spin-$\frac{1}{2}$ variables is described as follows:

$$\mathcal{H} = \sum_{j=1}^{N} h_j \sigma_j^z + \sum_{\langle j,k \rangle}^{N} J_{j,k} \sigma_j^z \sigma_k^z. \tag{2.6}$$

## 2.3 Exact Diagonalization

In the previous chapter we saw the relation between a QUBO problem and the Ising Hamiltonian; then being interested in optimizing the MP problem we have to find the ground state. At this point, one has to study the eigenvalue problem, i.e. solving the Time-Independent Schödinger Equation:

$$\mathcal{H}|\psi_i\rangle = E_i|\psi_i\rangle, \qquad \forall i = 1, \ldots, N. \tag{2.7}$$

In the case of Mission Planning the Hamiltonian is described as:

$$\mathcal{H} = \sum_{j=1}^{N} h_j \hat{\sigma}_j^z + \sum_{j>k}^{N} J_{j,k} \hat{\sigma}_j^z \hat{\sigma}_k^z + const. \tag{2.8}$$

Considering each lattice site has local base 2, since the are spin-$\frac{1}{2}$, for sizes $N < 30$ it is possible to use exact method, as exact diagonalization, to compute the ground state. In such cases, it is necessary to use an algorithm to address the eigenvalue problem. Commonly used algorithms include the *Power Method*, which begins from a random state and iteratively seeks the most significant eigenvalue, and the *QR algorithm* [30][31]. However, in certain situations, these algorithms may not be efficient in solving the eigenvalue problem when dealing with large matrices. An alternative solution is the *Lanczos Method*, which identifies the transformation from a general matrix to a tridiagonal form to effectively tackle the eigenvalue problem [32][12].
The Mission Planning Hamiltonian is a classical one, defined in real-space, whose size is $(2^N \times 2^N)$, and it is diagonal by constructions, which requires three terms to be built:

- constant term, which is equivalent to the first term of the Eq. 1.31;
- field term **h**, described by the second and third term of the Eq.1.31. This terms is an array of dimension $(1 \times N)$
- spins interaction term **J**, described by the last three terms of the Eq. 1.31. This term is a matrix of dimension $(N \times N)$ which is a symmetric matrix.

The main complex task involves constructing the Hamiltonian by summing over the variables, specifically $\mathcal{O}(N \cdot 2^{2N})$. When dealing with a classical Hamiltonian, one can explore the eigenstate by arranging the diagonal elements of the matrix in ascending order. This process enables the extraction of the system's energy spectrum, namely the eigenvalues.

## 2.4 Entanglement in Quantum System

Taking a generic state $|\psi\rangle$, one can use the *density matrix* formalism to extract information about the entanglement of the system.

$$\rho = |\psi\rangle\langle\psi|, \tag{2.9}$$

which has the following properties:

1. $\rho = \rho^\dagger$;
2. $Tr(\rho) = 1$;
3. $Tr(\rho^2) \leq 1$.

In the context of a quantum lattice system, where the lattice sites are divided into two sets $\mathcal{A}$ and $\mathcal{B}$, forming a bipartition of the system, the state of this system is denoted as $|\psi\rangle_{\mathcal{AB}}$. The density matrix of the system, $\rho_{\mathcal{AB}}$, is given by Eq.2.9. One can introduce the *reduced density matrix* as a way to characterize the system:

$$\rho_{\mathcal{A}} = \mathrm{Tr}_{\mathcal{B}}(\rho_{\mathcal{AB}}) = \sum_k \langle \mathcal{B}_k | \rho_{\mathcal{AB}} | \mathcal{B}_k \rangle, \tag{2.10}$$

which correspond to the partial trace with respect to the partition $\mathcal{B}$.
In this setting, a way to quantify the entanglement for quantum states, the *von Neumann* entropy, also known as the entanglement entropy, may be proposed. Considering a state $\psi$, described by its density matrix $\rho$, the von Neumann entropy of the subsystem $\mathcal{A}$ is defined as:

$$S(\rho_{\mathcal{A}}) = -\,\mathrm{Tr}[\rho_{\mathcal{A}} \log_2 \rho_{\mathcal{A}}] = -\sum_j \lambda_j \log(\lambda_j), \tag{2.11}$$

with $\lambda_j$ the $j$-th eigenvalue of $\rho_{\mathcal{A}}$.
To quantify entanglement in a system, a bipartition of the system into $\mathcal{A}$ and $\mathcal{B}$ must be applied. Computing the entanglement entropy of the reduced density matrix of one subsystem reveals whether the state is separable or not. Where, for a bipartite state $|\psi_{\mathcal{AB}}\rangle$ two orthonormal bases, $|\psi_{\mathcal{A},i}\rangle$ and $|\psi_{\mathcal{B},j}\rangle$, exist such that the state, $|\psi_{\mathcal{AB}}\rangle$, can be expressed as:

$$|\psi_{\mathcal{AB}}\rangle = \sum_i \lambda_i^{[\mathcal{AB}]} |\psi_{\mathcal{A},i}\rangle |\psi_{\mathcal{B},i}\rangle. \tag{2.12}$$

This decomposition is called the *Schmidt decomposition*, where the $\lambda_i^{[\mathcal{AB}]}$ are the *Schmidt-coefficient*. In practice, this decomposition can be achieved through the singular value decomposition (SVD), where the state can be expressed as $\phi = U\sigma V^\dagger$, where $\sigma$ is the matrix with the Schmidt coefficients, while $U$ and $V$ form the orthonormal basis.
Using the Schmidt decomposition, it is possible to quantify the entanglement between the two subsystems, $\mathcal{A}$ and $\mathcal{B}$, by the von Neumann entropy, which takes the form:

$$S(\rho_{\mathcal{A}}) = S(\rho_{\mathcal{B}}) = -\sum_i |\lambda_i^{[\mathcal{AB}]}|^2 \log\left(|\lambda_i^{[\mathcal{AB}]}|^2\right). \tag{2.13}$$

The number of nonzero Schmidt coefficients is also referred to as Schmidt rank. One may observe that the set of $\lambda_i$ corresponds to the eigenvalues of the reduced density matrix of the bipartition $\mathcal{A}$ ($\mathcal{B}$). This is called entanglement spectrum.

## 2.5 Tensor Network methods

The aim of this section is to introduce the *Tensor Network* (TN) methods for many body problems. Given a many-body quantum state, its complete representation contains all the available information and is described by $d^N$ parameters.

$$|\Psi\rangle = \sum_{\vec{\alpha}} c_{\alpha_1,\alpha_2,\ldots,\alpha_N} |\alpha_1\alpha_2\ldots\alpha_N\rangle.$$

A description of the state in terms of mean-field approximation reduces the number of parameters to $N$, which is described as:

$$|\Psi^{MF}\rangle = |\psi^1\rangle \otimes |\psi^2\rangle \otimes \cdots \otimes |\psi^N\rangle.$$

Tensor Network methods interpolates between these two representations of the many body wave function. On this representation on of the most prominent techniques to address many body systems is is the *Density Matrix Renormalization Group* (DMRG), pioneered by S. White in the 1990s[33][34]. The central concept revolves around executing the renormalization procedure within the density matrix eigenstate domain, rather than the real space. In doing so, all pertinent information, crucial for representing quantum many-body states, resides within the degrees of freedom associated with the entanglement of the quantum wave function. Tensor Network methods have demonstrated their efficacy in successfully addressing quantum many-body problems on classical computers. They achieve this by efficiently representing quantum many-body states, leveraging the inherent entanglement properties of the system. Other possible representations of a variational state are the *Matrix Product States* (MPS) [35], which employ Tensor Networks for addressing both equilibrium and out-of-equilibrium [36] problems in one-dimensional systems. *Multi-scale Entanglement Renormalization Ansats* (MERA) [37] offers an efficient representation tailored for critical systems, and *Tree Tensor Network* (TTN) [38], which can represent systems with high dimensionality.

### 2.5.1 Tensors Network: Definition

The concept underlying Tensor Networks revolves around efficiently parameterizing the wave function of a physical system using a network structure comprised of interconnected tensors. This network comprises tensors interconnected to encode information within the complex network. This arrangement significantly decreases the overall parameter count from an exponential $\mathcal{O}(e^N)$ to a polynomial $\mathcal{O}(poly(N))$. By decomposing a large tensor into multiple smaller tensors connected by additional indices referred to as *bond-links*, the number of links is dictated by the *bond-dimension* $\chi$. Increasing $\chi$ allows for better control over information retention in the Tensor Network. In practical terms, the bond-link that joins two tensors defines the entanglement structure in the quantum state, with the bond dimension quantifying the level of entanglement present. A tensor can be defined as follows:

**Tensor Definition**: A complex tensor $\mathcal{T} \in \mathbb{C}^{d_1 \times \cdots \times d_R}$ is defined as a dense R-dimensional array of complex numbers mapping the R-dimensional manifold to a complex scalar:

$$\mathcal{T} : \mathcal{V}_1 \times \cdots \times \mathcal{V}_R \longrightarrow \mathbb{C}. \tag{2.14}$$

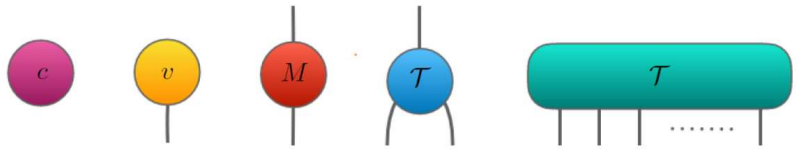


Figure 2.1: Graphical representation of a scalar $c \in \mathbb{C}$, a one-link tensor (i.e. a vector) $v \in \mathbb{C}^{d_1}$, a two-link tensor (i.e. a matrix) $M \in \mathbb{C}^{d_1 \times d_2}$, a three-link tensor $\mathcal{T} \in \mathbb{C}^{d_1 \times d_2 \times d_3}$ and a generic tensor of order R.[13]

Where, it becomes evident that a vector is equivalent to an order-1 tensor, a matrix is an order-2 tensor and a 3-order tensor is a three-dimensional array, and for each dimension there is associated a corresponding link. Typically, the overall count of indices in a tensor is called its *rank*, while its dimension aligns with the dimension of the vector space from which it originated. A standard representation of a tensor is as follows:

$$\mathcal{T}_{\alpha_1,\ldots,\alpha_N}.$$

Dealing with tensors that have multiple indices can be quite complex, but it can be made much

more manageable by representing each tensor operation as a tensor network. Viewing the manipulation of tensors in this way can be considered an extension of linear algebra.
Some of these manipulations are as follows:

- **Fusion**: combine adjacent tensor links into a single *fused-link*;
- **Splitting**: split the *fused-link* into the original links;
- **Contraction**: given two tensors, they can be combined over all shared links.

In quantum mechanics, Tensor Network states serve as representations of arbitrary pure quantum many-body states, denoted as $|\Psi\rangle$, in the Hilbert space $H$. Here, the lattice $\mathbb{L}$ is a D-dimensional lattice that encompasses $N$ sites. Each site $k \in [1,\ldots,N]$ is characterized by a local Hilbert space $H_k$ that has a finite dimension $d_k$. Consequently, the complete Hilbert space of $\mathbb{L}$ is spanned by $H = \otimes_{k=1}^{N} H_k$. The most comprehensive form of a pure state existing on such a lattice can be expressed as:

$$|\psi\rangle = \sum_{i_1=1}^{d_1} \sum_{i_2=1}^{d_2} \cdots \sum_{i_N=1}^{d_N} \Psi_{i_1,i_2,\ldots,i_N} |i_1\rangle \otimes |i_2\rangle \otimes \ldots |i_n\rangle, \tag{2.15}$$

where $|i_k\rangle$ denotes the local state of the site $k$. This gives $dim(\Psi) = d^N$. A Tensor Network shall be defined as a tuple $\mathcal{G} = (\mathbb{T},\mathbb{R})$ consisting of a set $\mathbb{T} = \{\mathcal{T}\}$ of two or more tensors and a set $\mathbb{R} = \{\alpha\}$ of corresponding links. The set $\mathbb{R}$ is divided into *internal* links connecting the tensors with each other and *external* or *physical* link which are connected to one tensor only.
Depending on how the complete state vector $\Psi_{i_1,i_2,\ldots,i_N}$ will be decomposed, it may be represented by various geometries. The most notable system configurations include the *Matrix Product State* (MPS), *Multi-scale Entanglement Renormalization Ansatz* (MERA) and *Tree Tensor Network* (TTN), which is the TN structure used for the purpose of this thesis.

#### 2.5.1.1 Bond Dimension and Area Law

An important role in the Tensor Network approach is given by the bond dimension $\chi$, which represents the dimension of the bond link connecting two tensors, and the underlying entanglement structure. From this perspective, breaking down a random state into a tensor network would require an exponentially large bond dimension to exactly depict the wave function. However, most physical quantum states adhere to specific entanglement bounds under real-space bipartition, a principle known as the *Area Law*. The area law of entanglement holds for ground states of local gapped Hamiltonians, where the interactions are limited to a finite range[39]. This restriction

ensures that entanglement between distant parts of the system decays rapidly. It states that for a ground state of a local gapped Hamiltonian, the amount of entanglement between two regions is proportional to the surface area that separates them, rather than the volume of either region individually. Then the entanglement entropy between two regions of a d-dimensional system scales ad: $S \sim l^{d-1}$[40]. However, there are exceptions to this rule. In certain systems with long-range interactions or unconventional symmetries, the entanglement entropy may exhibit behavior that deviates from the area law. For example, critical systems near a quantum phase transition may display logarithmic violations of the area law, where the entanglement entropy scales logarithmically with the volume of the subsystem. This principle enables the effective decomposition of such states into a tensor network, highlighting that the entanglement properties of tensor network states can be managed by the network's topology. Taking into account a pure state $|\Psi\rangle$ represented by a tensor network, the bipartition, $\mathcal{A}$ and $\mathcal{B}$, is made between the physical link, and then this network can be bipartitioned with respect to the two physical partitions by cutting through a set of internal links. Given this partition, the von Neumann entropy satisfies the following inequality:

$$S_{TN}^{[\mathcal{A},\mathcal{B}]} \leq \min_k \left[ \sum_i \log \chi_k \right]. \tag{2.16}$$

where $\chi_k$ is the bond dimension of the broken link $i_k$, i.e. the links in which the separation occurs. In other words, the network which represents the state is divided into two sub-networks. Every broken link can maximally give an entropy of $\log \chi_k$, upper-bounded by its bond dimension $\chi_k$.

### 2.5.2 Tree Tensor Network

A Tree Tensor Network (TTN) follows a hierarchical structure with different layers, where as shown in figure 2.2, the first layer $\Lambda_1$ consists of two tensors connected via the root-link, which is the topmost-link in the network, while the other tensors connected to these first layer come from the second layer $\Lambda_2$, and so on. In this structure, each tensor in layer $\Lambda_{l>1}$ has exactly one neighbour in layer $\Lambda_{l-1}$, which is defined as its *parent tensor*, and may have several neighbours in layer $\Lambda_{l+1}$ which are defined as its *child tensors*. The depth of a TTN is defined as the number of layers $\mathcal{L}$, that is, the longest path between a tensor and the root link.
Given that the computational complexity of contracting a network increases with the multipli-

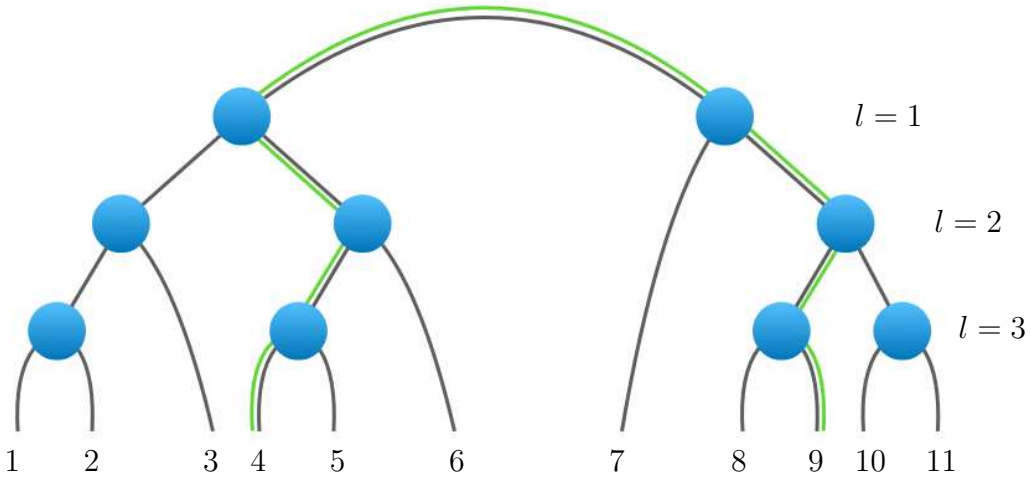


Figure 2.2: Structure of a general binary Tree Tensor Network, where the green line is the only possible path from tensor at position $4$ to tensor at position $9$[13]

cation of the bond dimensions of all connections linked to the tensors, it is advisable to reduce the number of connections per tensor in order to create a tensor network that can be contracted efficiently. Hence, a specific class of interest is the *binary* Tree Tensor Network (TTN), utilized for this thesis, wherein each tensor can have at most three neighbors, namely, two children in the hierarchical structure. In general, there are two categories of binary TTNs:

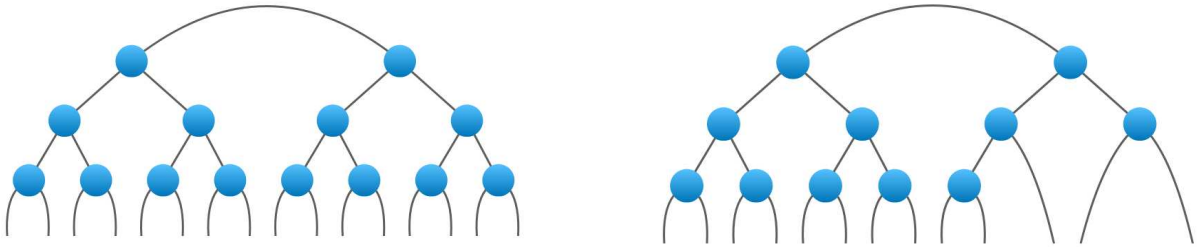

(a) (b)

Figure 2.3: Structure of a perfect TTN $(a)$ filled with $N = 2^{\mathcal{L}}$ tensors, and a complete TTN $(b)$.[13]

- **Perfect TTN**, as shown in Fig.2.3a, where each layer $l$ is completely filled with the maximum number of tensors, i.e. $2^l$. Each tensor with layer $\Lambda_{l<\mathcal{L}}$ has two child tensors, while the tensors within the last layer $\Lambda_{\mathcal{L}}$ have only one internal link connecting it to its parent tensor and two physical links that address the local Hilbert spaces of the system. Then this type of network is only able to capture system with $N = 2^{\mathcal{L}}$.
- **Complete TTN**, as shown in Fig.2.3b, as for the perfect TTN, each layer is completely filled, except for the last layer $\Lambda_{\mathcal{L}}$ which is filled form the left.

### 2.5.2.1 Ground-State Search on TTN

The results obtained in this thesis are based on the ground state search on a TTN as developed in Quantum Green Tea library [1]. In the following we briefly sketch the algorithm fo the optimization. This optimization capitalizes on the independence of each single tensor within the network, allowing them to be treated as individual variables. The fundamental concept in optimizing a tensor network state $|\psi\rangle$ involves optimizing one tensor at a time[41].
Now, let $\mathcal{H} \in H$ be the Hamiltonian of a quantum many-body system, and $\Psi$ a TTN to represent a wave function of the same Hilbert space. Then the ground state of $\mathcal{H}$ is the solution of the following minimization problem:

$$\min_{\Psi}\{E(\Psi)\} = \min_{\Psi}\{\langle\Psi|\mathcal{H}|\Psi\rangle\}, \tag{2.17}$$

the variational parameters of the TTN are then optimized to minimize the energy $E(\Psi)$. The TTN enables the optimization process by considering each tensor as a distinct set of variational parameters. The overall optimization is achieved through a process called *sweeping* across the network, which involves carrying out local optimizations. If we focus on optimizing a specific tensor, it involves holding the other tensors constant.

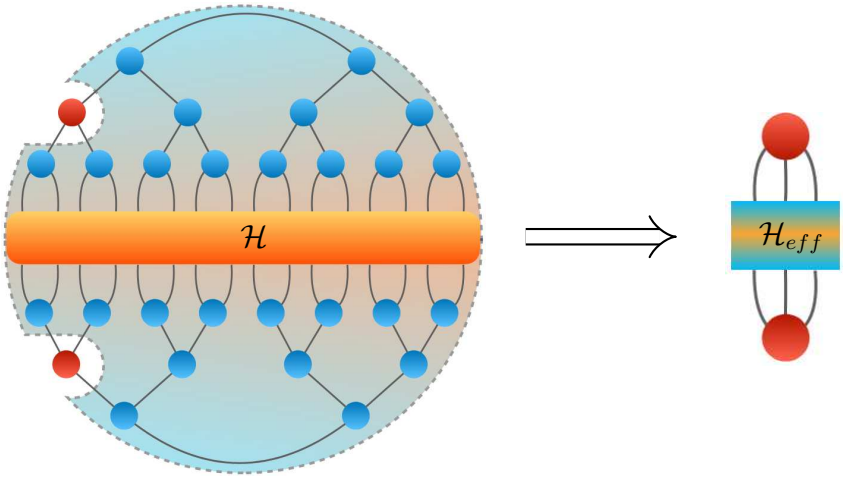


(a) (b)

Figure 2.4: Optimization to find the Ground state for a target tensor (red), (a)its environment (shaded area) is contracted into the effective Hamiltonian of the local problem. (b) Ending at an eigenproblem with $\mathcal{H}_{eff}$[13]

[1] https://www.quantumtea.it/

To conduct this local optimization, the Tensor Network can be differentiated with respect to any single arbitrary tensor $\mathcal{T}^i$:

$$\frac{\partial \Psi}{\partial \mathcal{T}^i} \equiv \Psi^i_{env}.$$

From this definition, the expected energy can be reformulate with respect to a single tensor:

$$E\left(\Psi\right) = \langle \Psi | \mathcal{H} | \Psi \rangle = \langle \mathcal{T}^i | \Psi^i_{env} \mathcal{H} {\Psi^i_{env}}^\dagger | \mathcal{T}^i \rangle = \langle \mathcal{T}^i | \mathcal{H}^i_{eff} | \mathcal{T}^i \rangle.$$

By contracting the Hamiltonian with all the other tensors in the network, a new tensor network emerges, which represents an eigenvalue problem for the selected tensor and the *effective* Hamiltonian $\mathcal{H}_{eff}$, as shown in Fig.2.4. Upon solving this eigenvalue problem, the selected tensor is replaced by the eigenvector corresponding to the lowest energy eigenvalue. This process, performed for all tensors in the network, constitutes a single *sweep* optimization. This procedure can be applied iteratively until convergence to the global ground state is achieved.

### 2.5.2.2 Local Observables

As for the Ground-State search, to compute an observable the procedure is quite similar. After the optimization of all tensors, it is possible to use the ground state to calculate the expected value of an observable.
An efficient way to achieve this expected value of a general observable, defined as:

$$\langle O^{[i]} \rangle_\psi = \langle \psi | O^{[i]} | \psi \rangle,$$

is to isometrize the TTN towards the selected tensor, which acts at the physical site $i$. Using this isometry, the computation of $\langle O^{[i]} \rangle_\psi$ can be executed by the contraction of the other tensors, as shown in Fig.2.5 [41], with a complexity of only $\mathcal{O}(d^3 m) + \mathcal{O}(d^2 m)$ where $d$ is the local dimension of the physical system.

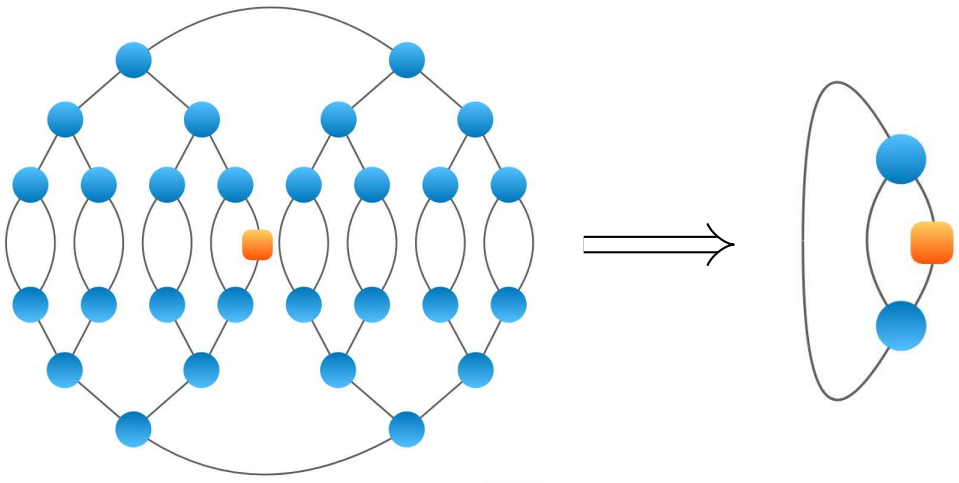

(a) (b)

Figure 2.5: Contraction scheme for the computation of an expected value of a local observable (orange block) acting on a generic site (a). Isometrising the network toward the tensor directly connected to the operator simplifies the computation to a contraction of three tensors (b), since the other tensors act as isometries and effectively become an identity when contracted with their corresponding complex conjugate.[13]

# 3 Results

*In this chapter, the mission planning problem is analyzed from the perspective of the TTN approach. Before detailing how to access the optimal solution, we describe the numerical generation of a pool of Mission Planning instances Sec.3.1. In Sec.3.2, some features of the Mission Planning Hamiltonian will be highlighted. Finally, in Sec.3.3, the key results achieved are presented, detailing the different strategies adopted to improve the quality of the results.*

## 3.1 MP instance generation and reconstruction of the optimized mission

In this Section we construct a set of optimization problems characterized by random values of parameters such as acquisition, download and preparation times, and an increasing number of optimization variables. Since realistic MP instances are not available for this study, we generate this dataset of problems randomly. We generate a certain number of instances for each system size, with time parameters randomly drawn from a uniform probability distribution within the range of values specified in Table 3.1, as indicated by TASI, see Chapter 1. Overall, the total number of variables considered is defined as:

$$N_{tot}^{var} = \sum_{i=1}^{N} \sum_{j=1}^{M} \theta_{i,j} + M \sum_{i=1}^{N} \sigma_i,$$

For simplicity, since the TTN ansatz consists of a number of physical sites that is a power of two, we deal with variables that can also be expressed as powers of two. Therefore, each particular instance describes a specific mission to be optimized, characterized by certain random parameters that impose a certain number of constraints on the minimization of the cost function, as elaborated in detail in Sec.1.3.

| **Mission Planning instance** | | | |
|---|---|---|---|
| Parameter ID | Description | Domain | Range Values |
| N | number of satellites | $\mathbb{N}$ | [2-10] |
| M | number of ARs | $\mathbb{N}$ | [2-15] |
| $\theta_{i,j}$ | number of DTOs | $\mathbb{N}$ | [2-5] |
| $\sigma_i$ | number of DLOs | $\mathbb{N}$ | [2-5] |
| $t_{i,j}^k$ | Instant acquisition time | $\mathbb{R}$ | [1hr-24hr] |
| $s_{i,j}^r$ | Instant downlink time | $\mathbb{R}$ | [1hr-24hr] |
| $p_{i,j}^k$ | Preparation time after one acquisition | $\mathbb{R}$ | [1hr-4hr] |
| $d_{i,j}^k$ | Preparation time after one downlink | $\mathbb{R}$ | [1hr-4hr] |

Table 3.1: This table reports the range values and the domains of the randomly generated parameters, used to create a set of MP instances to be studied applying the methods explained in chap.2

Once the MP instance dataset is obtained, we construct the corresponding ground-state search problem for each random instance as described in Chapter 2. At this point, it is important to clarify that the outcome obtained from the TN variational ground-state search requires additional post-processing to determine the quantities of interest of the original optimization problem, namely the optimal planned mission and the corresponding cost. The optimized plan is described by a sequence of $0s$ and $1s$ representing the values of the decision variables, referred to as the MP *bitstring*, along with its associated cost obtained by substituting the optimal values of the DTO and DLO binaries directly into the cost function of Eq. 1.30. Specifically, the outcome of the TN variational optimization is an approximation of the true ground state of the many-qubit system. This state encodes a given MP instance along with its corresponding en-

ergy.

The strategy we adopt to reconstruct the optimal mission from the TTN ground state is as follows: we compute the expectation value of the spin-1/2 operator corresponding to each site of the 1D chain where the qubits are arranged, i.e., we compute the quantum average over each site given by

$$\langle\psi|\hat{\sigma}_i^z|\psi\rangle, \tag{3.1}$$

where,

$$\hat{\sigma}_i^z = \mathbb{1} \otimes \cdots \otimes \mathbb{1} \otimes \underset{\text{i-th}}{\hat{\sigma}_z} \otimes \mathbb{1} \otimes \cdots \otimes \mathbb{1}. \tag{3.2}$$

In the quantum mapping, the expectation value of each operator represents the optimal value of the single binary variable of the original problem. Once we obtain this expectation value for each site, which will be either $+1$ or $-1$, we use the mapping from spin variables to binary variables to reconstruct the complete MP bitstring.

Subsequently, having reconstructed the optimal mission plan, it is possible to calculate its cost directly from the cost function (Eq. 1.1), which can be compared with the outcomes of classical solvers to evaluate the effectiveness of this approach, see Sec.3.3. Furthermore, apart from reconstructing the MP bitstring and evaluating its associated cost, an equally significant metric in this context is the "quality" of the optimized mission. This quality is quantified by the number of constraints fulfilled by the optimized mission relative to the total number of constraints in the cost function minimization, see Sect.1.4. Once the MP bitstring is identified, its quality can be assessed by verifying that all equations and inequalities are met. This can be done by substituting the binary values into the equations and inequalities and then counting the number of constraints that are satisfied. The ratio of constraints satisfied to the total number can be expressed as a percentage. Therefore, if the bitstring satisfies all the constraints, its quality will be $100\%$, otherwise it will be lower.

Another important factor is the arrangement of the MP variables, which define the 1D chain of the MP Hamiltonian. The choice of variable ordering could significantly influence the search for the ground state since the arrangement of the 1D chain determines how the local tensors are connected to each other. In this case, the variables ordering consists of the DTO variables followed by the DLO variables, with respect to the target. The variables order representing the 1D chain is as follow:

$$\Big[\underbrace{\tau^1_{1,1},\tau^2_{1,1},\nu^1_{1,1}}_{\text{1st target}},\ldots\ldots,\underbrace{\tau^1_{i,j},\ldots\tau^k_{i,j},\nu^1_{i,j},\ldots\nu^r_{i,j}}_{j\text{-th target}},\ldots\ldots,\underbrace{\tau^1_{N,M},\ldots\tau^k_{N,M},\nu^1_{N,M},\ldots\nu^r_{N,M}}_{\text{M-th target}}\Big].$$

## 3.2 Features of MP Hamiltonian

Before presenting the results of applying Tensor Network methods to solve the MP instances outlined in the preceding section, we initially illustrate certain characteristics common to these instances by examining small-size cases. This is done to offer insight into the problems we aim to solve and to visually demonstrate where the difficulty in optimizing these tasks lies. We recall that the spin-glass Hamiltonian encoding each instance has the following form:

$$\mathcal{H} = \sum_{j=1}^{N_{tot}^{var}} h_j \hat{\sigma}_j^z + \sum_{j>k}^{N_{tot}^{var}} J_{j,k} \hat{\sigma}_j^z \hat{\sigma}_k^z, \tag{3.3}$$

where $N_{tot}^{var}$ is the number of spins (qubits) in the systems and the longitudinal magnetic field $h_j$, and the couplings $J_{j,k}$ of the spin-spin interactions contain the information regarding a specific instances to be solved, as explained in sec.1.4.

When constructing an MP Hamiltonian, the offset term in Eq.1.31 is set aside, since it is identical for all terms. Instead, the spin-glass couplings $h_j$ and $J_{jk}$ are adjusted to a range of $[-1, 1]$ for numerical efficiency. These adjustments do not affect the exploration of the ground state and can be incorporated after the optimization process. However, the Hamiltonian spectrum does not correspond to the mission cost and requires further processing.

One of the challenges in solving this type of Hamiltonian lies in the long-range nature of spin-spin interactions. In general, **J** is a symmetric matrix, and the distances between two interacting spins are typically greater than one, meaning spins beyond nearest neighbors can interact with each other. An example is the interaction matrix **J** for an MP instance with 16 binary variables represented in Fig.3.1, where the long-range interactions and the symmetric structure are evident. It is also noted that the majority of the long-range interactions involve binary variables describing the acquisition and/or the downloading of the same target identified by the index $j$. This aspect is characteristic of the optimization problem we are considering in this thesis and justifies the choice of ordering DLO and DTO qubits along the 1D chain on which to build the TTN ansatz.

Another important aspect to highlight is that although the MP Hamiltonian 3.3 is diagonal, finding its ground state is complicated due to the presence of a large number of local minima, which is a peculiar feature of glassy systems [42]. This extremely rugged energy profile makes the search for the global minima difficult because during the optimization there is a high probability of getting stuck in a local minimum depicted as a very narrow valley from which it is challenging to escape, as shown in figure 3.2 for a very small instances with 8 qubits.

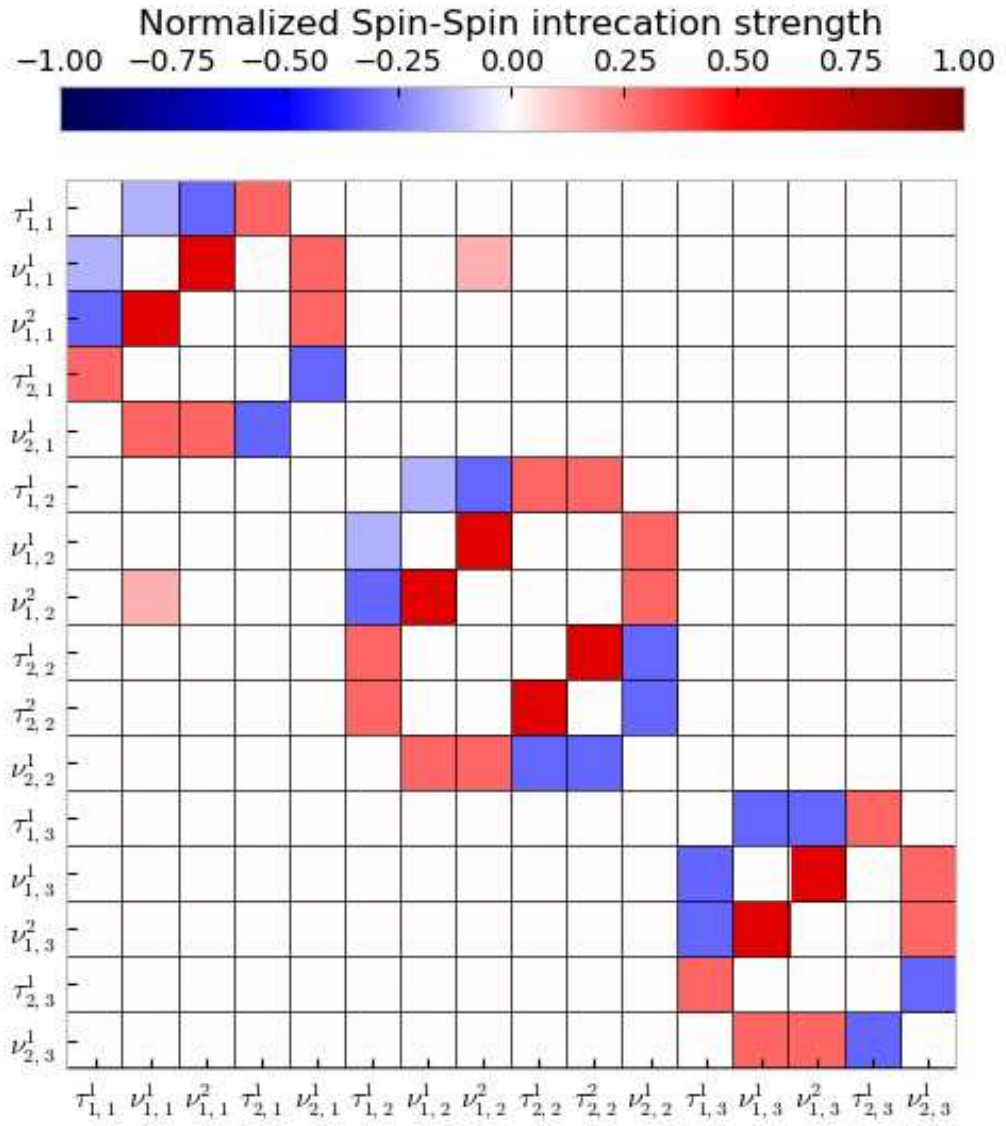


Figure 3.1: The color map represents the matrix **J**, which takes values in $[-1,1]$, for a 16 variables instance, with 7 DTOs and 9 DLOs. On the axes are reported the DTO and DLO variables, $\tau^k_{i,j}$ and $\nu^r_{i,j}$. Every square corresponds to a matrix element that reflects the interaction among the spin variables indexed on the row and column. The white squares indicate the absence of interactions between the column spins and the row spins, whereas the colored ones depict the interaction terms that define a specific instance.

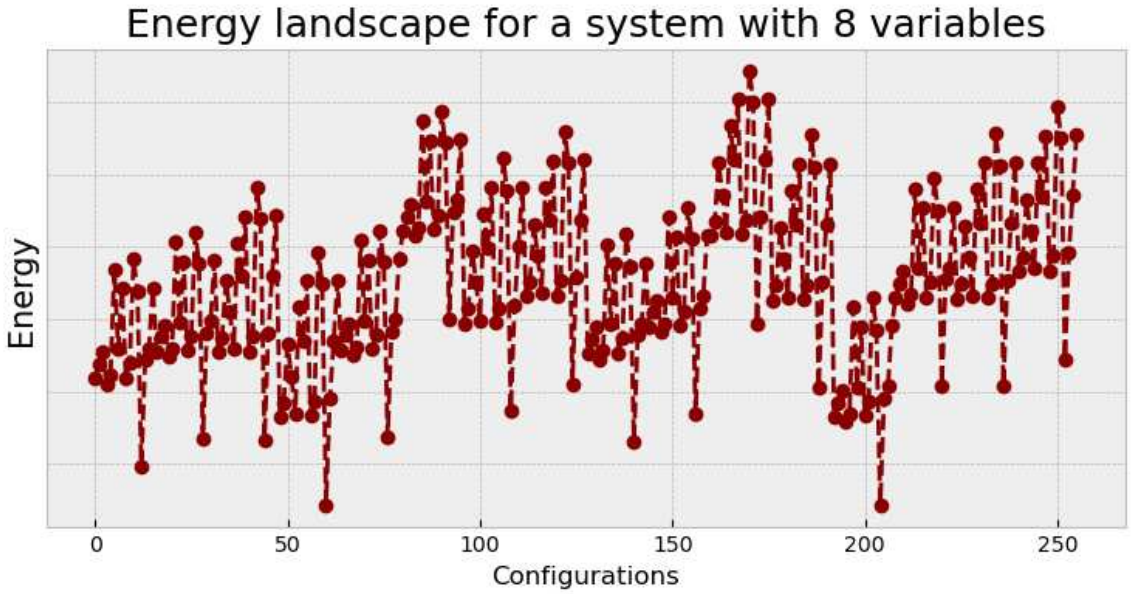


Figure 3.2: Spectrum energy landscape of the MP Hamiltonian for all possible configurations, for an 8 qubits instance, with $2^8$ possible configurations over which to search for the ground state. In the y-axis it is represented the Hamiltonian energy, and in the x-axis there are the possible configurations of the spins orientation.

One implication of this profile is that the outcomes produced by the selected algorithm could significantly vary based on the initial setup for the optimization process. A key objective of this study is to investigate whether the TTN approach can overcome this issue or is affected by it, and in case, to understand which strategy can be adopted to overcome this issue, as it will be discuss in the following sections.

## 3.3 Tree Tensor Network approach

In this section we report and discuss the results obtained by solving the MP Hamiltonians via Tree Tensor Network (TTN) ground-state search algorithm.

### 3.3.1 TTN energy convergence

A fundamental numerical analysis in evaluating a TN-based approach involves studying the energy convergence during the tensors optimization (see Chapter 2) as a function of the bond dimension, which is the main control parameter in this type of variational ansatz. Understanding the energy convergence of the TTN allows us to assess the scaling of the bond dimension with the problem size increases. To this end, we consider three different random instances characterized by three different problem sizes.

- **16 qubits** system, composed with 7 DTOs and 9 DLOs;
- **32 qubits** system, composed with 16 DTOs and 16 DLOs;
- **64 qubits** system, composed with 36 DTOs and 28 DLOs.

In Figure 3.3, we display the absolute value of the relative energy difference compared to the exact ground-state energy. By exact ground-state energy, we mean the energy obtained by explicitly writing the matrix representing the Hamiltonian operator and identifying the smallest value along the diagonal in the case of 16 qubits. For the other two instances, characterized by a number of qubits that cannot be tackled using exact techniques, we computed this energy through a TTN ground-state search - as implemented in the Quantum Green TEA library - considering a very large bond dimension, $\chi = 300$ for the 32 qubits instance and $\chi = 180$ for the 64 qubits instance. We emphasize that in the limit of infinite bond dimension, the TTN provides an exact but inefficient representation of the system's wave function.

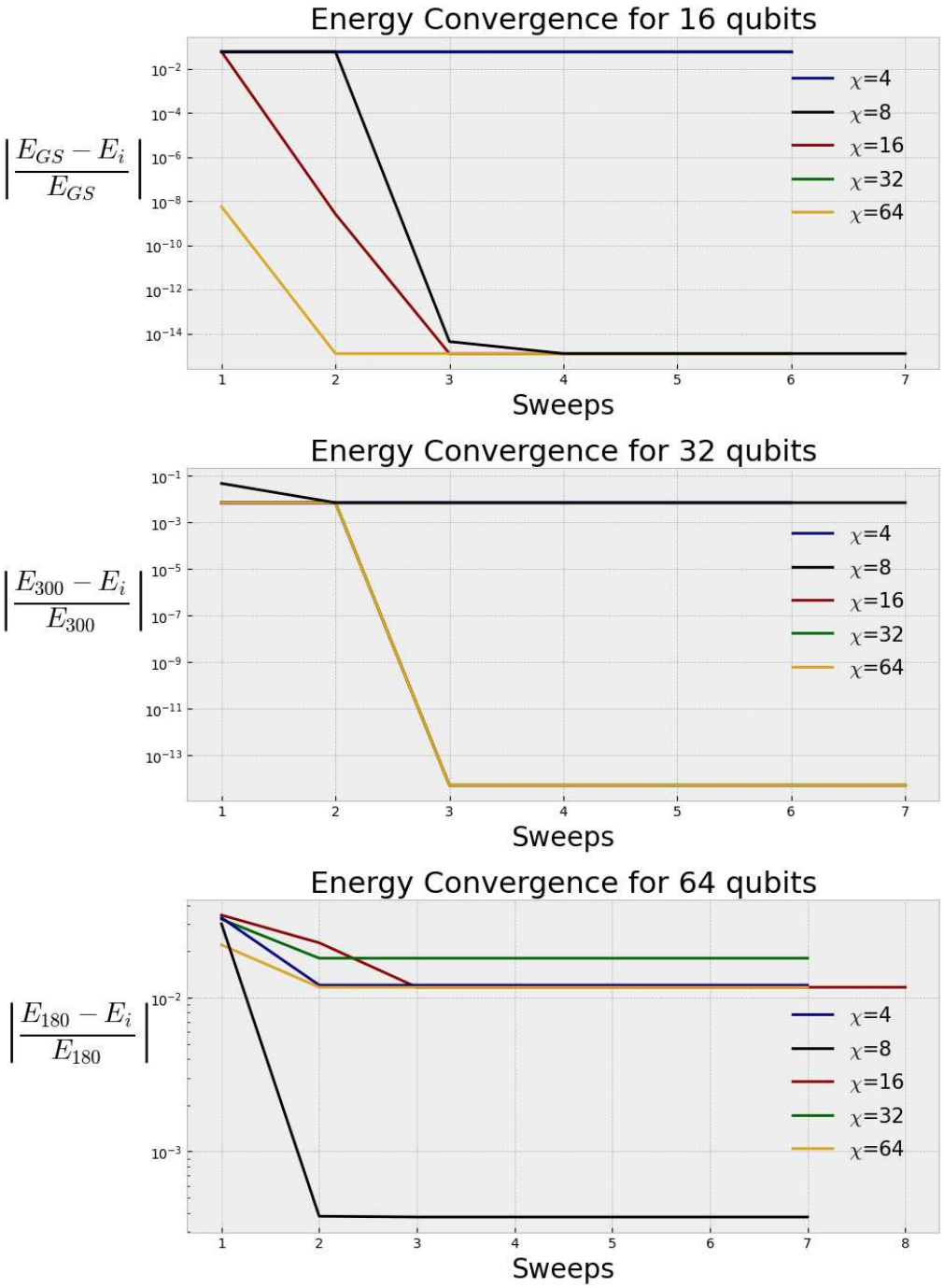


Figure 3.3: TTN energy convergence as a function of the sweeps for different values of the bond dimension. In the y-axis there is the absolute value of the relative energy with respect to the exact diagonalization (16 qubits case) and TTN ground-state search with the largest possible bond dimension in the case of 32 and 64 qubits, with $\chi = 300$ and $\chi = 180$, respectively. In the 16 qubits case, the blue and black lines corresponding to bond dimensions 4 and 8 overlap. For 32 qubits, the yellow and green lines ($\chi = 32$,64) overlap and the other three corresponding to bond dimensions 4,8,16 overlap each other.

We observe that, the larger bond dimension, the quicker the energy convergence. This does not apply to the case of 64 qubits, where the best results are obtained with $\chi = 8$ possibly as a result of the random initialization of the algorithm. However, as we will observe in the following sections, the outcomes from this instance display a particular behavior.
The parameters used to quantify whether the energy converged - as they appear into the *TNConvergenceParameters* class of the Quantum Green tea library - are: absolute and relative deviations that establish the convergence threshold, the number of check points where the deviations are evaluated, and the maximum number of sweeps to prevent non-converging energy behavior. The values assigned to these parameters are shown in table 3.2.

| **Convergence Parameters** | |
|---|---|
| max_iter | 30 |
| abs_deviation | $10^{-9}$ |
| rel_deviation | $4 \cdot 10^{-9}$ |
| n_points_conv_check | 5 |

Table 3.2: Convergence Parameters for ground-state search, applied to the TTN optimization algorithm of the Quantum Green Tea library. The max_iter is the maximum number of sweeps, useful to prevent non-converging energy behavior. The abs_deviation is the absolute deviation threshold, rel_deviation is the relative deviation threshold; if the values of these deviation computed over the number of check points are smaller than the thresholds the optimization is stopped. The n_points_conv_check are the number in which the deviations are computed.

### 3.3.2 Escaping local minima using random transverse fields

As mentioned in sec.3.2, the spectrum of an MP Hamiltonian is characterized by a large number of local minima, and given that the optimization starts selecting a random initial state, it can be intuitive to understand that depending on the chosen random state, the optimization could get stuck in a local minimum. A possible approach to avoid this problem is to include an additional factor in the Mission Planning Hamiltonian, a local *transverse field*. The idea is to introduce a new term that non-commutes with the MP Hamiltonian, where the intensity of the transverse field is several orders of magnitude smaller than the coupling term **J** which describes the MP Hamiltonian. In a first approximation, we expect that the energy spectrum order will not be modified. At this point, the new Hamiltonian reads as follows:

$$\mathcal{H}_{MP} + 10^{-\xi} \sum_{i=1}^{N_{var}^{tot}} q_i \sigma_i^x, \tag{3.4}$$

where **q** is a random array in $[-1,1]$, $\sigma_x$ is the the x-component of the Pauli matrices, and $\xi$ is a parameter to be tuned.

To understand whether the presence of this field can affect the convergence to better minima, the energy convergence with different weights for the transverse field is studied. The study was carried out showing the convergence of the energy density, which is the energy of the system divided by the number of spins, of three systems with different sizes ($N_{var}^{tot} = 32,64,128$), setting the bond dimension $\chi$ to 64. In the following figure 3.4, the convergence of the energy density is shown in the presence of a transverse field with different weights. For different-sized instances, the transverse field affects in different ways; to have significant changes in the ground state search the magnitude of the transverse field must be increased with respect to the system size. For the following analysis, when the transverse field is taken into account, the magnitude of it will be $10^{-7}$ for all 32 qubits systems, $10^{-5}$ for the 64 ones, and $10^{-4}$ for the systems at least with size 128; according to the figure.

At this point, figure 3.5 shows, for the 64 qubits system, the differences between the energy convergence of the previous cases with different bond dimensions, and the convergence applying the transverse field with the selected order of magnitude ($10^{-5}$) and bond dimension $\chi$ set to 64. As displayed, the application of this field helps to achieve a better minima. In this case, the presence of the transverse field leads us to consider it as a potentially optimal strategy. However, in the following section, additional analysis are conducted to verify its effectiveness.

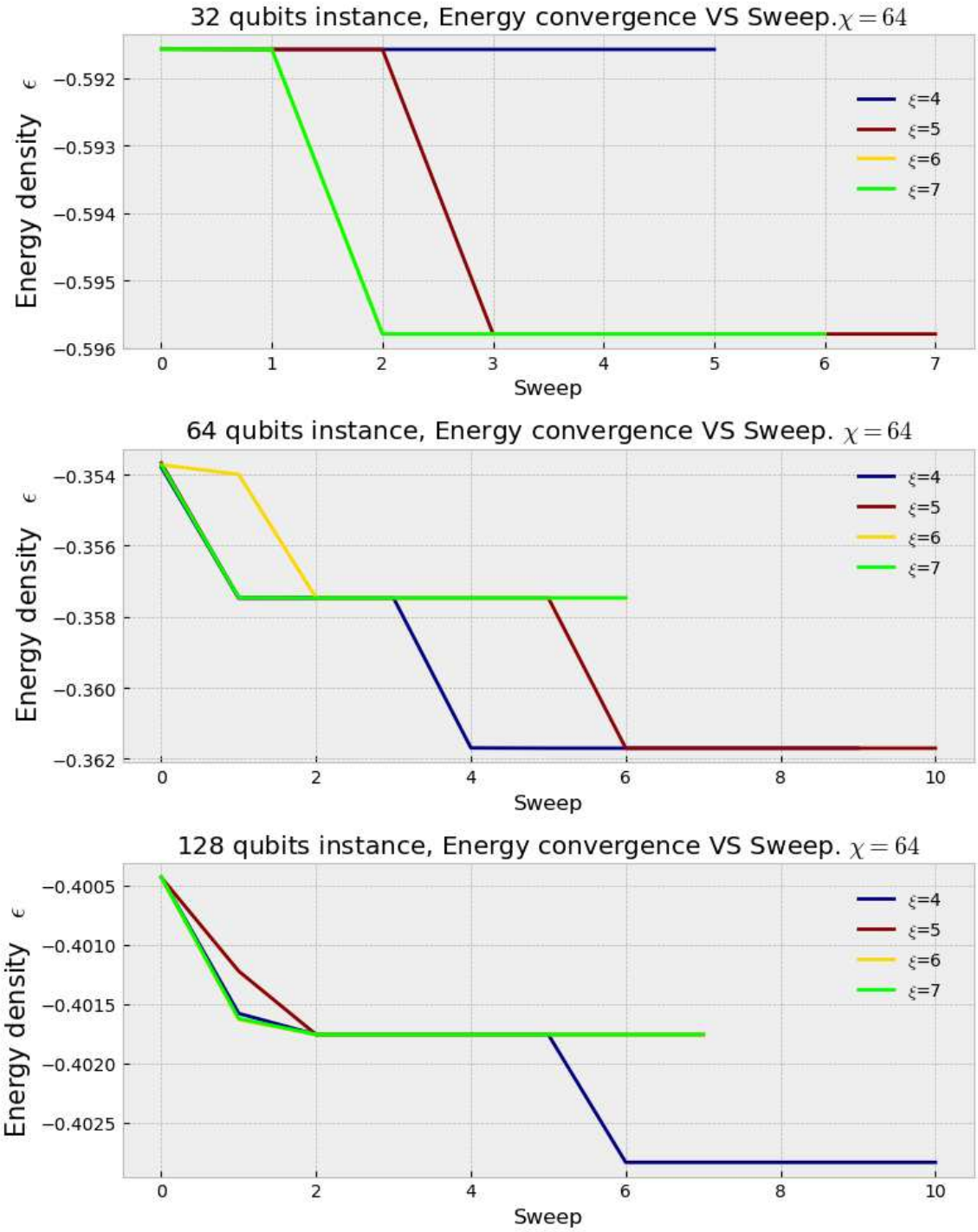


Figure 3.4: Energy density convergence during sweeps progression for three different-sized instances with different weights of Transverse field. In the x-axis there are the sweeps required to achieve the convergence. In y-axis is shown the energy density, which is the Energy of the state divided by the number of qubits. The trends show that with the increasing of the system size the $\xi$ factor have to be decrease to find a better solution.

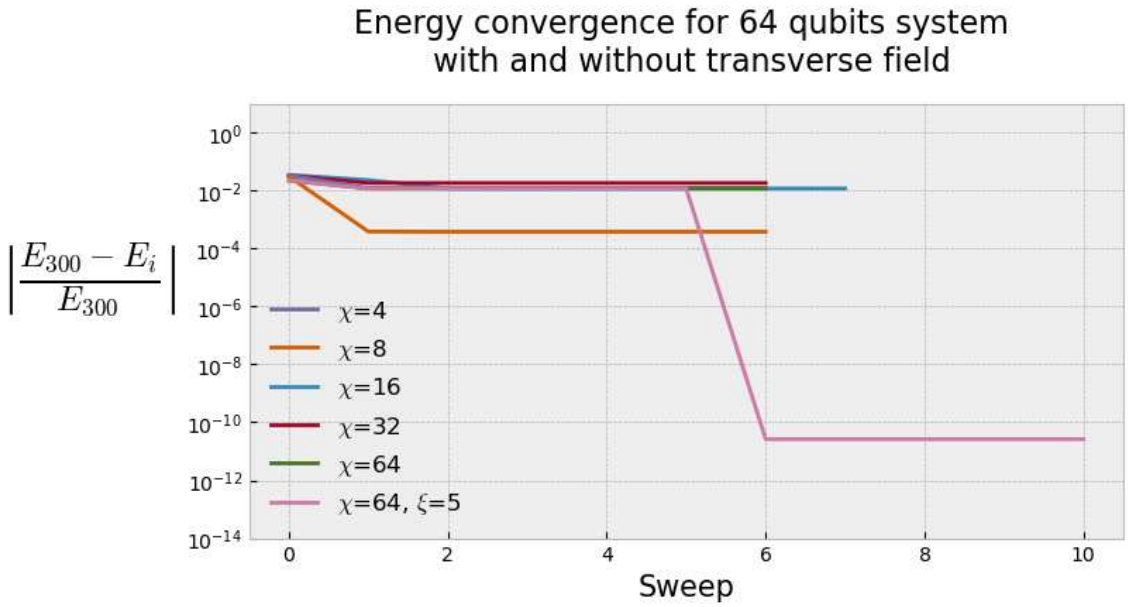


Figure 3.5: Energy convergence during sweeps progression for the 64 qubits system, considering the cases without transverse field and with transverse field, with the chosen order of magnitude ($10^{-5}$). In the y-axis there is the relative energy compared to the ground state energy computed with $\chi = 300$. In the x-axis there are the required sweeps to complete the convergence process in according to the convergence parameter explaind in table3.2. The transverse field added to the Hamiltonian shows a clear improvement.

### 3.3.3 Random Inizialization

As stated in the preceding subsection, the TTN approach, to solve an eigenvalue problem, start the optimization from a random state. To see how random initialization influences the optimization, the ground-state search of a given system is made iterating over different random initializations. This approach can give an important result on how the bond dimension and the transverse field affect the optimization. To illustrate these results, we define a *frequency*, which means the number of times the optimization reaches the reference ground state. The first analyzed system is the one with N=32.

In figure 3.6, the frequency of the found ground state is shown for different bond dimensions and different number of random initializations for the initial state. The energy of the ground-state to which it is compared is computed with a high bond dimension ($\chi = 300$) and the transverse field with $\xi = 7$. From the figure, it is evident that in this case the bond dimension plays a crucial role in finding the ground state: when the bond dimension is too small, the algorithm does not reach the target ground-state. In the case of $\chi = 2^0$, which represent a factorized state, even realizing $10^5$ different initializations out of the $2^{32}$ possible configurations, the TTN algorithm does not

reach the ground state even once. Then, applying a higher bond dimension, which increases the quantum correlations represented, the frequency of found ground state increases. We observe that, with at least a bond dimension $\chi = 16$, the probability to access the reference ground-state is $\sim 0.9$. Contrarily, the presence of the transverse field does not seem to show any substantial advantage.

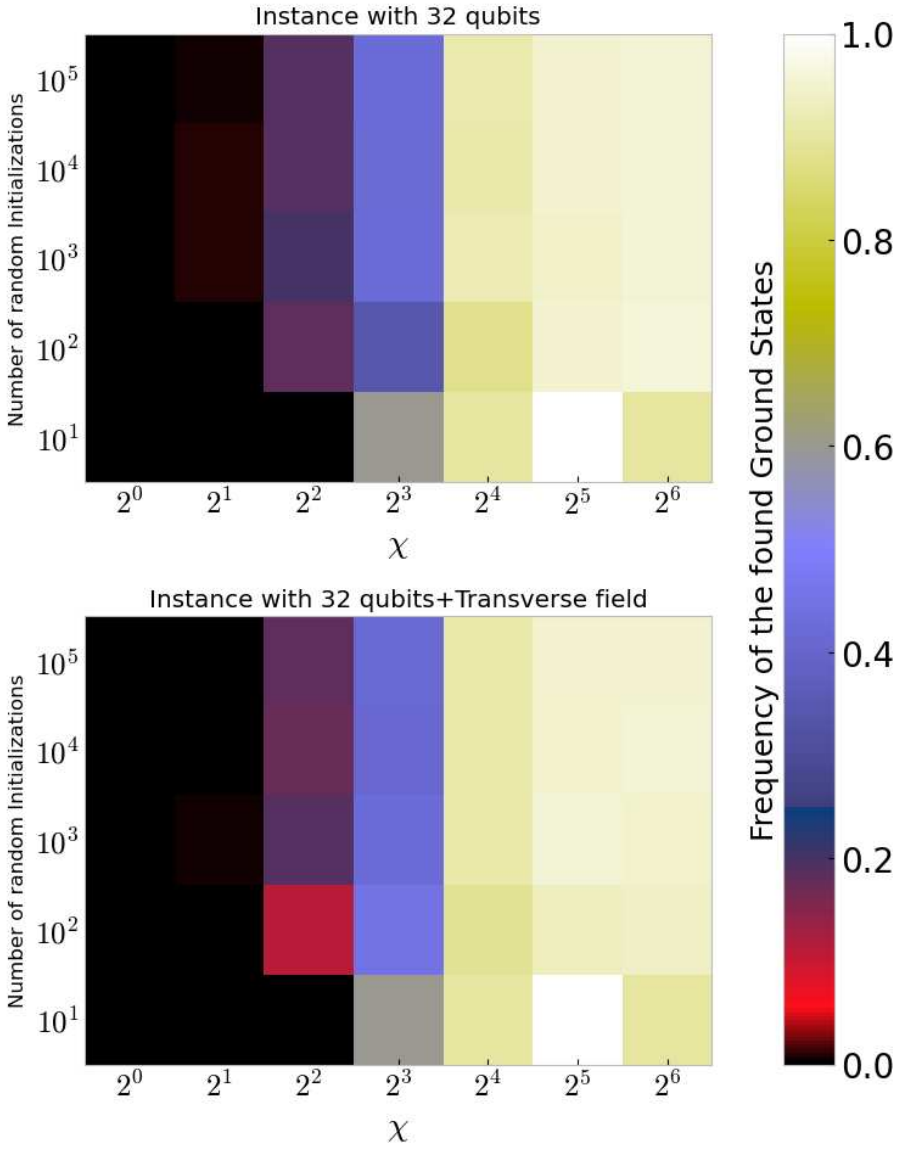


Figure 3.6: Random initializations with (bottom) and without (upper) transverse field for different bond dimensions, in the case of a 32 qubits system. The color bar represents the frequency, which defines the number of time the target ground state is reached. For this case the most significant parameter is the bond dimension. In the x-axis there is the bond dimension, and in the y-axis there are the number of random initializations. In the color bar, the black represent only the $0.0$ value. The order of magnitute of the transverse field is $10^{-7}$.

We consider now larger instances. Taking into account a system with 64 qubits with different random initializations, the reference ground state energy is computed by setting $\chi = 180$, and transverse field $\xi = 5$. In figure 3.7, the frequency of the ground state is shown for different random initializations, with and without transverse field.

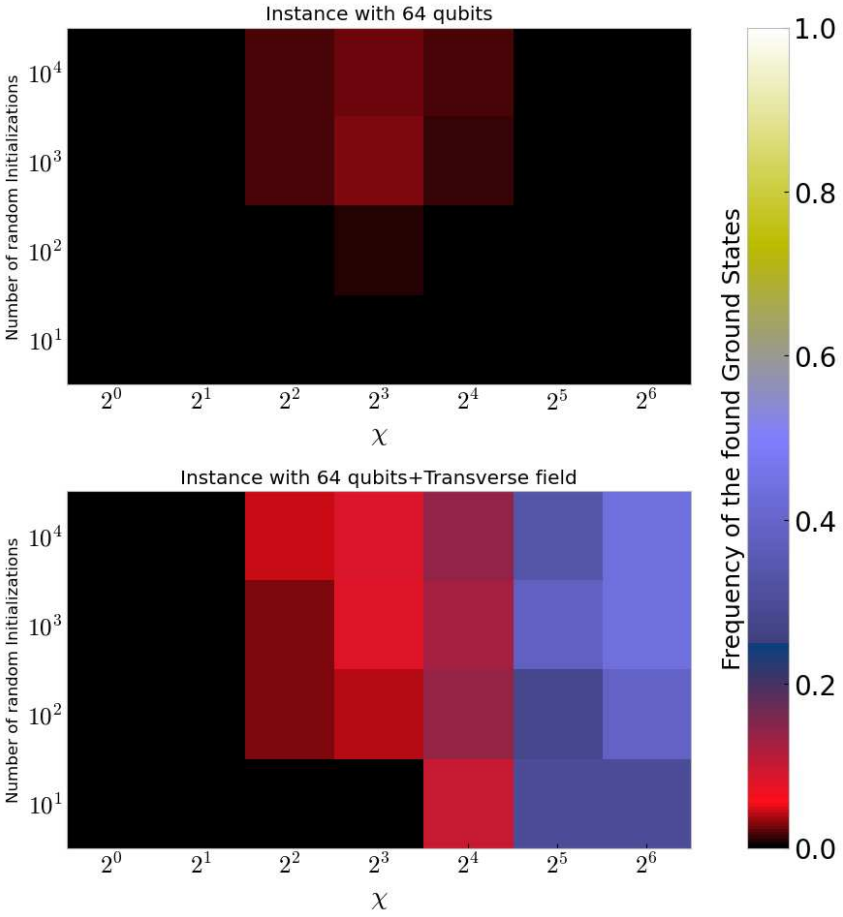


Figure 3.7: Random initializations with (bottom) and without (upper) transverse field for different bond dimensions, for 64 qubits system. Showing the frequency of found ground state. The bond dimension does not affect the optimization if the transverse filed is not present. In the x-axis there is the bond dimension, and in the y-axis there are the number of random initializations. In the color bar, the black represent only the $0.0$ value.The order of magnitude of the transverse field is $10^{-5}$.

Differently from the previous 32 qubits case, in the 64 qubits system the transverse field are playing a crucial role. Without the transverse field, even increasing the bond dimension does not have any affects, and it is almost impossible to reach the target ground state, even with $10^4$ different initializations, reporting a probability smaller than $0.1$. But looking at the bottom figure in 3.7 the transverse field increases the probability to $\sim 0.5$, with $\chi \geq 32$, compared to the

result without this field there is a clear improvement of the optimization, but it is not significant enough.

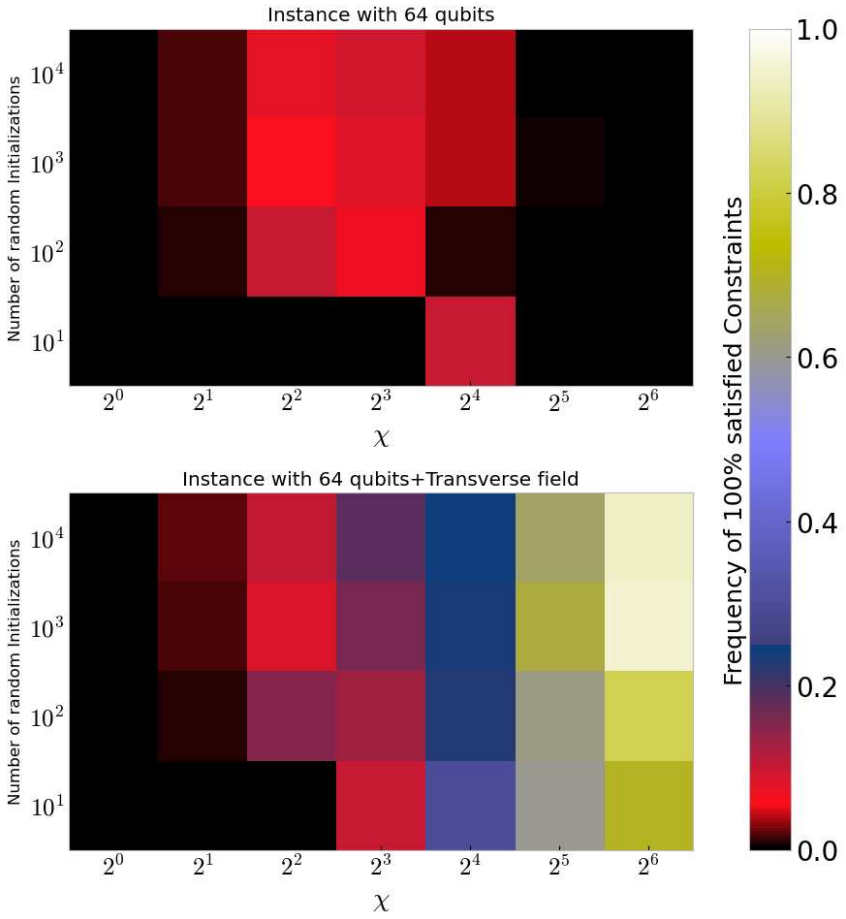


Figure 3.8: Frequency of 100% satisfied constraints. Random initializations with (bottom) and without (upper) transverse field for different bond dimensions, for a 64 qubit system.The order of magnitude of the transverse field is $10^{-5}$. In the x-axis there is the bond dimension, and in the y-axis there are the number of random initializations. In the color bar, the black represent only the 0.0 value.

In the context of the MP problem, the goal is to optimize the cost function while taking various constraints into account. Then, it could exist alternate missions that satisfy all the specified constraints. In this case, the energy difference between two mission plans, both 100% accurate, would be due to the different DTOs and DLOs variables used to satisfy the mission. At this point, we can focus on the mission quality by changing the metrics used to evaluate the algorithm efficiency into the frequency of 100% satisfied constraints. The term "satisfied constraint" refers to the percentage of indices in the entire bit string that meet the given constraints. In figure 3.8 we show the previous scenario with a different metric. The figure illustrates that, using a metrics based on the quality of the mission, the 64-qubit system has multiple feasible combinations that

meet all the specified constraints, however this metric shows clear changes compared to the previous cases. In the presence of a transverse field, there is a probability of around $0.8$ to find a solution that satisfies all constraints when $\chi = 64$. But in the case where there is no transverse field, the results are still poor: even with the increasing the bond dimension, the algorithm is able to find not even one solution satisfying all the constraints. One possible answer to this behavior could be that during the optimization we get stuck in a local minima which does not satisfy the $100\%$ of the constraints. To understand if this is the case, in figure 3.9, there is shown the same analysis of before with the only difference that the metrics is based on satisfying at least the $98\%$ of the constraints.

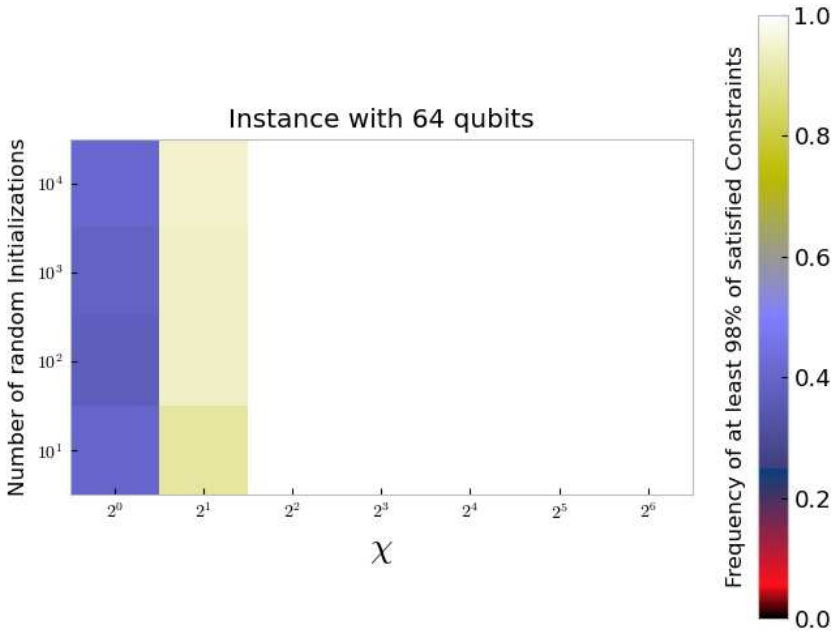


Figure 3.9: Frequency of at least $98\%$ satisfied constraints. Random initializations without transverse field for different bond dimensions, for a 64 qubit system. The optimization ends up getting stuck in a local minima. In the x-axis there is the bond dimension, and in the y-axis there are the number of random initializations. The with color in the color bare represents the frequency equal to $1.0$

However, it seems that even if we increase the bond dimension, one can at most satisfy $98\%$ of the constraints.

### 3.3.4 Comparison with a classical solver

We now focus on the qualities of the mission plans in terms of satisfied constraints. To have a general overview of how the algorithm behaves, different instances are taken into account, with dimensions: $32, 64, 128, 256, 512$ and $1024$. Approximately $20$ random instances have been generated, as explained in Sec.3.1, for each of these dimensions. We emphasize that since these instances are generated using random parameters, it is impossible to determine in advance if there is a solution that fulfills all the specified constraints. To have a comparison with the TTN algorithm, we use here a classical solver to assess the mission quality. The solver used is the *CPLEX* algorithm, developed by Robert E. Bixby and now owned by IMB (incorporated into the Qiskit library) [43], is a high-performance mathematical programming solver for integer programming problems, and convex quadratic constrained problems.

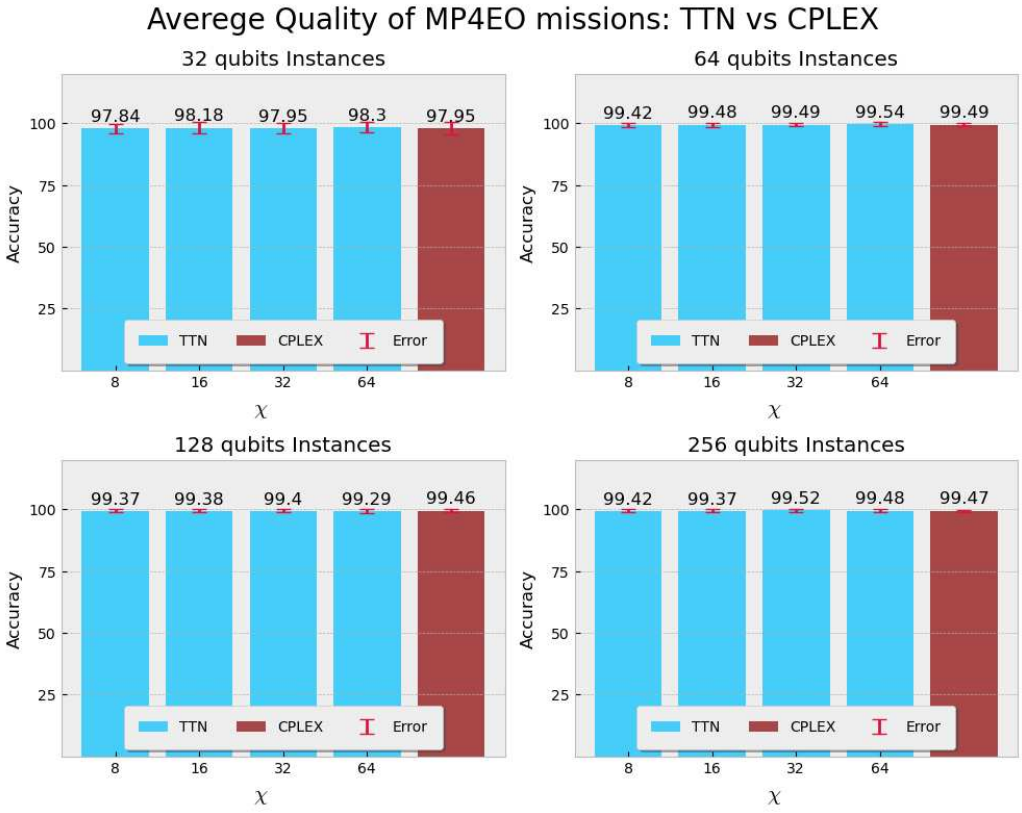


Figure 3.10: Comparisons of the mission accuracy between the TTN with different bond dimensions (blue) and the CPLEX solver (brown). In the x-axis there are the bond dimension for the TTN optimizer, in the y-axis there is the mean accuracy of the missions, computed over different instances, with their errors.

Starting with system sizes from 32 to 256 qubits, Figure 3.10 shows histograms, where each blue bar corresponds to the mean accuracy across all instances of a given dimension, for different bond dimensions. The brown bar represents the mean of the quality of the solution obtained by the CPLEX solver. By comparing the cases with bond dimension $\chi = 64$ to the results obtained with CPLEX, the percentage of the satisfied constraint is approximately equal or better for the TTN case.

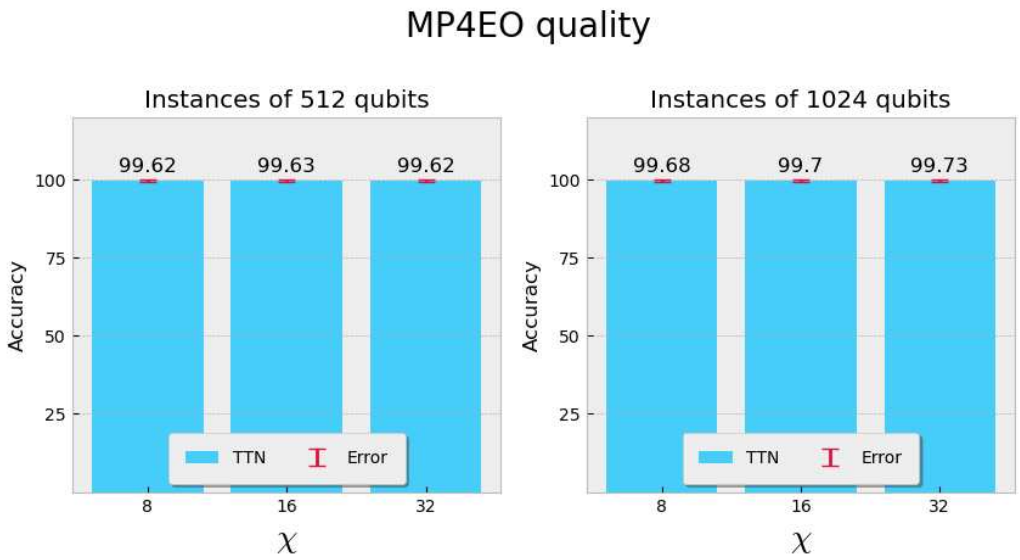


Figure 3.11: Mission accuracy for system with 512 and 1024 qubits, applying the TTN optimization algorithm, In the x-axis there are the bond dimension for the TTN optimizer, in the y-axis there is the mean accuracy of the missions, computed over different instances, with their error. The TTN algorithm shows a stable quality of the output even with the increasing of the system size.

To understand how the TTN optimizer behaves with the increasing of the system size, the same analysis is done for $512$ and $1024$ qubits. In figure 3.11, the mean accuracy of the mission plan is shown for different bond dimensions. In this case, it was not feasible to compare the outcomes with the CPLEX solver due to a size limit over the licence-free software. Moreover, due to limitations in time and memory, conducting a ground state search with a higher bond dimension has been challenging for all instances with 512 and 1024 qubits. Considering the accuracy shown in the figure, even with small bond dimension, the optimization is able to reach $99.7\%$ of the satisfied constraints. This is a very good result, considering the stability of the missions quality with the instance size.

Another important factor is the computational time to reach the optimal solution. Figure 3.12 shows the time required to find the optimal solution with the TTN algorithm as compared to

the CPLEX solvers. In the range of the explored instance sizes, the time needed by CPLEX is clearly better than the TTN optimization. Then for system with a small number of variables, such as from 32 to 256, CPLEX returns an optimal solution in terms of satisfied constraints, as like the TTN, but has an improvement on the computational time. On the contrary, without the ability to show the performance of the CPLEX solver on larger systems, it is difficult to determine which optimizer is more effective, especially considering the favorable results of the TTN approach on systems with 512 and 1024 qubits.

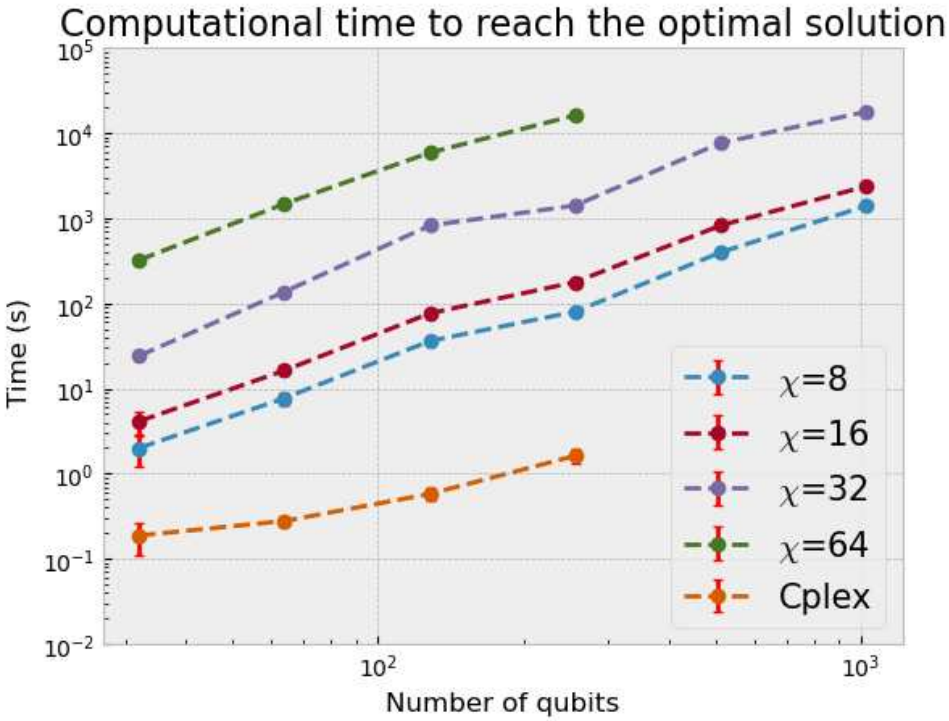


Figure 3.12: Computational time: TTN vs CPLEX. In the x-axis there is the number of qubits shown in logarithmic scale. In the y-axis there is shown the computational time to reach the optimal solution. For the studied system with the CPLEX solver it shows a better scalability in terms of time.

# 4 Conclusions

In this thesis, we employed Tensor Network (TN) methods from the Quantum Green TEA library to investigate the Mission Planning (MP) problem numerically. This problem, central to Earth Observation (EO), is pivotal for understanding our planet's state, encompassing the analysis of atmospheric events and climate change impacts. Firstly, we outlined the MP problem in EO, where the ultimate goal is coordinating satellite activities to acquire and download Earth surface images efficiently. Mathematically, we formulated this complex task as a Quadratic Program (QP), aiming to minimize a suitable cost function under feasibility constraints.

From the QP formulation, we rephrased the MP problem into the ground-state search of a corresponding many-qubit system, making it amenable to TN methods. This entailed constructing the Quadratic Unconstrained Binary Optimization (QUBO) problem, integrating constraints into the cost function as quadratic penalty terms. Furthermore, we implemented a post-processing strategy to circumvent the introduction of additional optimization variables. After obtaining the QUBO for a generic MP instance, we mapped binary variables to spin-$1/2$, yielding the Ising spinglass Hamiltonian describing long-range interacting spins. Subsequently, we promoted spin variables to quantum operators representing qubits, resulting in a many-body Hamiltonian that can be studied using TN-based numerical techniques.

We efficiently searched for the ground state by representing the system's wavefunction as a Tree Tensor Network (TTN). Exploring the convergence to the ground-state energy with different bond dimensions on random MP problem instances, we observed a significant reliance on tensor initialization. Moreover, we found that the variational ground-state search algorithm can get stuck in local minima characterizing the energy landscape of this hard optimization problem, particularly evident in instances with $64$ qubits.

To address this issue, we introduced additional transverse field terms to escape local minima, leveraging their non-commutativity with the problem's Hamiltonian. We showed that by adjusting the magnitude of these terms, energy convergence can be improved.

We then explored how the random initialization of TTN tensors impacts the number of optimal missions with energy matching the reference ground-state energy. We conducted this

analysis with and without transverse field terms in the Hamiltonian at different bond dimensions. This underscores the importance of the transverse field in optimizing quantum systems, especially in the $64$-qubit setup. Unlike smaller systems, it plays a critical role, significantly impacting our ability to achieve the desired state. Furthermore, we shifted our focus to prioritizing meeting all constraints rather than solely optimizing the cost function, as various combinations of variables can satisfy constraints, leading to differing energy levels between mission plans. Results indicate that the transverse field significantly enhances the probability of finding solutions meeting all constraints in the $64$-qubit system. Conversely, without it, outcomes are less favorable.

Finally, we extended our simulations up to instances with $1024$ qubits. For system sizes between $32$ and $256$ qubits, we compared TTN with results from the CPLEX classical solver. TTN with a bond dimension of $64$ showed comparable or superior constraint satisfaction percentages to CPLEX. However, for larger instances ($512$ and $1024$ qubits), direct comparison with CPLEX was hindered by software and computational limitations. Despite this, TTN achieved up to $99.7\%$ constraint satisfaction even with small bond dimensions. Yet, CPLEX proved more computationally efficient for smaller systems. Comparing their effectiveness for larger systems remains challenging due to unavailable CPLEX data. Nevertheless, TTN demonstrated promising results for systems with $512$ and $1024$ qubits, suggesting its potential in large-scale quantum optimization problems.

Future directions worth exploring for the TTN approach to the MP problem include incorporating additional constraints into the QUBO, such as considering memory limits for satellite data acquisition, devising better strategies to escape local minima, and comparing with classical solvers the performance of the TTN optimization of real-case problem instances relevant to the EO aerospace sector.

# Bibliography


[1] A. Lucas, “Ising formulations of many np problems,” *Frontiers in Physics*, vol. 2, 2014, issn: 2296-424X.

[2] S. Martello, D. Pisinger, and P. Toth, “Dynamic programming and strong bounds for the 0-1 knapsack problem,” *Management Science*, vol. 45, no. 3, pp. 414–424, 1999. (visited on 03/22/2024).

[3] Y. Akcay, H. Li, and S. Xu, “Greedy algorithm for the general multidimensional knapsack problem,” *Annals of Operations Research*, vol. 150, pp. 17–29, Mar. 2007.

[4] P. J. Kolesar, “A branch and bound algorithm for the knapsack problem,” *Management Science*, vol. 13, no. 9, pp. 723–735, 1967. (visited on 03/22/2024).

[5] A. Caprara, H. Kellerer, U. Pferschy, and D. Pisinger, “Approximation algorithms for knapsack problems with cardinality constraints,” *European Journal of Operational Research*, vol. 123, no. 2, pp. 333–345, 2000.

[6] C. P.C. and B. J.E, “A genetic algorithm for the multidimensional knapsack problem,” *Journal of Heuristics*, vol. 4, pp. 63–68, Jun. 1998.

[7] A. Drexl, “A simulated annealing approach to the multiconstraint zero-one knapsack problem,” *Computing*, vol. 40, no. 1, pp. 1–8, 1988.

[8] F. Hembecker, H. S. Lopes, and W. Godoy, “Particle swarm optimization for the multidimensional knapsack problem,” in *Adaptive and Natural Computing Algorithms*, B. Beliczynski, A. Dzielinski, M. Iwanowski, and B. Ribeiro, Eds., Berlin, Heidelberg: Springer Berlin Heidelberg, 2007, pp. 358–365.

[9] A. Bayerstadler, G. Becquin, J. Binder, *et al.*, “Industry quantum computing applications,” *EPJ Quantum Technology*, vol. 8, Dec. 2021.

[10] M. A. Nielsen and I. L. Chuang, *Quantum Computation and Quantum Information: 10th Anniversary Edition*. Cambridge University Press, 2010.

[11] M. Schuld, I. Sinayskiy, and F. Petruccione, "An introduction to quantum machine learning," *Contemporary Physics*, vol. 56, no. 2, pp. 172–185, Oct. 2014.

[12] M. Simone, *Introduction to Tensor Network Methods*. Springer International Publishing, 2018.

[13] T. Felser, "Tree tensor networks for high-dimensional quantum systems and beyond," Ph.D. dissertation, University of Padova, University of Saarland, 2021.

[14] ESA, *Observing the earth*, https://www.esa.int/Applications/Observing_the_Earth/View_from_above, 2022.

[15] EUSPA, *Observing the earth*, https://www.euspa.europa.eu/european-space/eu-space-programme/what-earth-observation, 2023.

[16] G. Zhang, X. Li, G. Hu, Z. Zhang, J. An, and W. Man, "Mission planning issues of imaging satellites: Summary, discussion, and prospects," *International Journal of Aerospace Engineering*, 2021.

[17] H. Kellerer, U. Pferschy, and D. Pisinger, *Knapsack Problems*. Jan. 2004.

[18] F. Glover, G. Kochenberger, and Y. Du, *A tutorial on formulating and using qubo models*, 2019.

[19] G. Kochenberger, J.-K. Hao, F. Glover, *et al.*, "The unconstrained binary quadratic programming problem: A survey," *Journal of Combinatorial Optimization*, vol. 28, Jul. 2014.

[20] M. Lewis and F. Glover, *Quadratic unconstrained binary optimization problem preprocessing: Theory and empirical analysis*, 2017.

[21] E. Boros, P. Hammer, and G. Tavares, "Preprocessing of unconstrained quadratic binary optimization," *RUTCOR Research Report*, Jan. 2006.

[22] E. Farhi, J. Goldstone, S. Gutmann, J. Lapan, A. Lundgren, and D. Preda, "A quantum adiabatic evolution algorithm applied to random instances of an np-complete problem," *Science*, vol. 292, no. 5516, pp. 472–475, Apr. 2001.

[23] A. Das and B. K. Chakrabarti, "Colloquium: Quantum annealing and analog quantum computation," *Reviews of Modern Physics*, vol. 80, no. 3, pp. 1061–1081, 2008.

[24] F. Barahona, M. Grötschel, M. Jünger, and G. Reinelt, "An application of combinatorial optimization to statistical physics and circuit layout design," *Operations Research*, vol. 36, no. 3, pp. 493–513, 1988, issn: 0030364X, 15265463. (visited on 03/03/2024).

[25] F Barahona, "On the computational complexity of ising spin glass models," *Journal of Physics A: Mathematical and General*, vol. 15, no. 10, p. 3241, 1982.

[26] E. Boros and P. L. Hammer, "The max-cut problem and quadratic 0–1 optimization; polyhedral aspects, relaxations and bounds," *Annals of Operations Research*, vol. 33, pp. 151–180, 1991.

[27] E. Boros and P. Hammer, "Pseudo-boolean optimization," *Discrete Applied Mathematics*, vol. 123, pp. 155–225, Nov. 2002.

[28] K. Binder and A. P. Young, "Spin glasses: Experimental facts, theoretical concepts, and open questions," *Rev. Mod. Phys.*, vol. 58, pp. 801–976, 4 1986.

[29] S. F. Edwards and P. W. Anderson, "Theory of spin glasses," *Journal of Physics F: Metal Physics*, vol. 5, no. 5, p. 965, 1975.

[30] J. G. F. Francis, "The QR Transformation A Unitary Analogue to the LR Transformation—Part 1," *The Computer Journal*, vol. 4, no. 3, pp. 265–271, Jan. 1961.

[31] V. Kublanovskaya, "On some algorithms for the solution of the complete eigenvalue problem," *USSR Computational Mathematics and Mathematical Physics*, vol. 1, no. 3, pp. 637–657, 1962.

[32] C. Lanczos, "An iteration method for the solution of the eigenvalue problem of linear differential and integral operators," *Journal of Research of the National Bureau of Standard*, vol. 45, p. 2133, 1950.

[33] S. R. White, "Density matrix formulation for quantum renormalization groups," *Phys. Rev. Lett.*, vol. 69, pp. 2863–2866, 19 1992.

[34] S. R. White and D. A. Huse, "Numerical renormalization-group study of low-lying eigenstates of the antiferromagnetic s=1 heisenberg chain," *Phys. Rev. B*, vol. 48, pp. 3844–3852, 6 1993.

[35] A Klümper, A Schadschneider, and J Zittartz, "Matrix product ground states for one-dimensional spin-1 quantum antiferromagnets," *Europhysics Letters (EPL)*, vol. 24, no. 4, pp. 293–297, Nov. 1993.

[36] G. Vidal, "Efficient classical simulation of slightly entangled quantum computations," *Physical Review Letters*, vol. 91, no. 14, Oct. 2003.

[37] G. Vidal, "Entanglement renormalization," *Phys. Rev. Lett.*, vol. 99, p. 220 405, 22 2007.

[38] P. Silvi, V. Giovannetti, S. Montangero, M. Rizzi, J. I. Cirac, and R. Fazio, "Homogeneous binary trees as ground states of quantum critical hamiltonians," *Physical Review A*, vol. 81, no. 6, Jun. 2010.

[39] M. B. Hastings, "Solving gapped hamiltonians locally," *Physical Review B*, vol. 73, no. 8, Feb. 2006.

[40] L. Amico, R. Fazio, A. Osterloh, and V. Vedral, *Entanglement in many-body systems*, 2008.

[41] P. Silvi, F. Tschirsich, M. Gerster, *et al.*, "The tensor networks anthology: Simulation techniques for many-body quantum lattice systems," *SciPost Physics Lecture Notes*, Mar. 2019.

[42] P. Hauke, H. G. Katzgraber, W. Lechner, H. Nishimori, and W. D. Oliver, "Perspectives of quantum annealing: Methods and implementations," *Reports on Progress in Physics*, vol. 83, no. 5, p. 054 401, May 2020, issn: 1361-6633.

[43] IBM, *Ibm ilog cplex optimization studio*, https://www.ibm.com/products/ilog-cplex-optimization-studio.